ABSTRACT

RAPPLEYE, DEVIN SPENCER. Developing Safeguards for Pyroprocessing: Detection of Plutonium Co-deposition on a Solid Cathode in an Electrorefiner by Applying the Signature-Based Safeguards Approach. (Under the direction of Dr. Man-Sung Yim and Dr. Korukonda L. Murty).

Pyroprocessing is a promising technology for the reprocessing of spent nuclear fuel (SNF). One of its claimed benefits is its resistance to proliferation. However, as with any separation of SNF, it is not completely immune to the diversion of special nuclear material (SNM). Thus, safeguards need to be applied to pyroprocessing to prevent the diversion of SNM. However, traditional methods of material control and accountancy cannot feasibly be applied with current technology, largely due to the inability to precisely determine input quantities of SNM from the spent fuel. Thus, alternative methods need to be developed to track and confirm the flow of SNM for pyroprocessing. A prominent feature in some of the proposed safeguarding methods is an accurate process model of pyroprocessing. One of the more complex process units to model is the electrorefiner due to the many phenomena occurring. The performance of an electrorefiner model is examined for the detection of plutonium co-depositing on a solid cathode. The effect of the plutonium-to-uranium ratio and the exchange current density (EXCD) on the co-deposition of plutonium and the accompanying indicators are examined.

Using the model, a depressed cathode potential and an elevated cell current are indentified as potential indicators of the co-deposition of plutonium. Both of these are affected by the composition of the electrolyte in the electrorefiner and the EXCD which is a physical property of the electrorefining system. While affected by the EXCD, the amount of plutonium deposited on the cathode does not show a significant difference with varying EXCD values at the engineering-scale. On the other hand, the EXCD introduces an error in

the prediction of the cathode potential that could result in inaccurate and untimely detection of plutonium deposition on the cathode.

A model is developed that predicts the deposition rates at the cathode without complete knowledge of the compositions in the electrorefiner by using the values of the cathode potential at different requested cell current values. Although the model uses rough estimates of parameters, the predicted composition and deposition rate values and trends are consistent with ERAD. The model provides a theoretical basis for the method of signature-based safeguards for pyroprocessing. Accuracy of the model can be improved by better characterization of each species' reaction area, mass-transfer coefficient, EXCD and activity coefficient with respect to its concentration.

Developing Safeguards for Pyroprocessing: Detection of a Plutonium Co-deposition on Solid Cathode in an Electrorefiner by Applying the Signature-Based Safeguards Approach

by
Devin Spencer Rappleye

A thesis submitted to the Graduate Faculty of
North Carolina State University
in partial fulfillment of the
requirements for the degree of
Master of Science

Nuclear Engineering

Raleigh, North Carolina

2013

APPROVED BY:

_____	_____
Dr. Man-Sung Yim Committee Co-Chair	Dr. Korukonda L. Murty Committee Co-Chair
_____	_____
Dr. David N. McNelis	Dr. Michael F. Simpson
_____	_____
Dr. Jun Li	Dr. Jason M. Haugh

DEDICATION

To Joslyn, her many sacrifices have allowed me to achieve this milestone.

BIOGRAPHY

Devin, raised in South Jordan, Utah, graduated from Bingham High School in 2003. During high school, he served in student government as a vice-president of the student body. After graduating, he spent two years serving a mission for the Church of Jesus Christ of Latter-day Saints in Lithuania. In 2010, he graduated with a B.S. in Chemical Engineering from Brigham Young University. This combination of political, international and technical experience led him to this work in nuclear fuel cycles and non-proliferation.

ACKNOWLEDGMENTS

A special thanks to the following individuals and organizations who contributed to this work:

- Dr. Man-Sung Yim for advising me despite being in South Korea. He has sacrificed many odd hours of the days to consult me here, in North Carolina.
- Dr. Korukonda L. Murty for accommodating this long-distance advisement by providing on-site advisement.
- Dr. Michael F. Simpson for invaluable technical advisement and insights on safeguards and pyroprocessing. His contributions to this work are irreplaceable.
- Dr. David N. McNelis for support and guidance on the research process. His foresight and experience helped me avoid many pitfalls.
- Dr. Jun Li for technical assistance in model selection, modification and development.
- Riley Cumberland for his patience while familiarizing me with ERAD.
- Robert Hoover for his introduction to the modeling efforts of pyroprocessing.
- Dr. Supathorn Phongikaroon and Robert Hoover for their technical review during the development of the model in this work.
- The Russell Family Foundation for funding this work.
- My wife, Joslyn, for her patience as my work has crept into evenings, weekends and has sometimes taken me away from the home for days at a time.
- My Heavenly Father for His support, guidance and strength.

TABLE OF CONTENTS

LIST OF TABLES

LIST OF FIGURES

LIST OF SYMBOLS

Symbol	Meaning	Symbol	Meaning
A	Electrode surface area	j	Species
a	activity	k	Reaction rate constant
C	Concentration	N	Molar flux
D	Diffusion coefficient	n	Electrons transferred
d	Electrode diameter	R	Universal Gas Constant
E	Electrode potential	r	Reaction rate
F	Faraday's constant	Re	Reynolds number
h	Mass-transfer coeffient	T	Temperature
I	Current	Sc	Schmidt number
i	Current density	Sh	Sherwood number
Greek			
α	Transfer coefficient	η	Overpotential
γ	Activity coefficient	ν	Stoichiometric coefficient
δ	Diffusion layer thickness	ω	Rotational velocity of electrode
Superscripts			
a	Anode	o	Standard
c	Cathode	s	Surface
Subscripts			
c	Concentration	k	Current step/setting
eq	Equilibrium	o	Exchange
f	Forward	op	Operational
j	Reduced species	r	Reverse
j^{n+}	Oxidized species	s	Surface

LIST OF ABBEVIATIONS

AFCI	Advanced Fuel Cycle Initiative
ANL	Argonne National Laboratory
B-V	Butler-Volmer
CRIEPI	Central Research Institute of Electric Power Institute
DA	Destructive Analysis
EBR-II	Experimental Breeder Reactor – II
ER	Electrorefiner
ERAD	Enhanced REFIN with Anodic Dissolution
EXCD	Exchange Current Density
FCF	Fuel Cycle Facility
FP	Fission Products
HEU	Highly Enriched Uranium
HFEF	Hot Fuel Examination Facility
HLW	High-level waste
IAEA	International Atomic Energy Agency
IFR	Integral Fast Reactor
INL	Idaho National Laboratory
KAERI	Korea Atomic Energy Research Institute
LEU	Low-Enriched Uranium
MC	Megacoulombs
MC&A	Material Control and Accountability
MOX	Mixed-Oxide
NDA	Non-Destructive Assay
OCP	Open-Circuit Potential
PCR	Plutonium-to-Curium Ratio
PUR	Plutonium-to-Uranium Ratio
PRIDE	PyRoprocess integrated Inactive DEmonstration
PUREX	Plutonium – Uranium Extraction
SNF	Spent Nuclear Fuel
SNM	Special Nuclear Material
SQ	Significant Quantity
TRU	Transuranic
UI	University of Idaho
UNC	University of North Carolina

1 Introduction

Pyroprocessing is a promising technology for reprocessing spent nuclear fuel (SNF). At the core of the process is the electrolysis of transuranics, specifically uranium and plutonium, from SNF. The process of the separation of materials via electrolysis is referred to as electrorefining. It has yet to be employed for industrial purposes. However, the U.S., South Korea, Japan and India are actively researching pyroprocessing [1, p. 1]. One of the advantages of pyroprocessing over the traditional reprocessing technology, PUREX, is the prevention of pure plutonium separation which is the material of concern for nuclear proliferation. However, it is not completely immune to the diversion of special nuclear material (SNM). Operational conditions of pyroprocessing can be altered to divert the flow of plutonium. Domestically at Idaho National Laboratory (INL), Material Control and Accountability (MC&A) – the tracking of SNM inventory in a process – has been applied to an engineering-scale pyroprocessing operation for treatment of spent fuel from the Experimental Breeder Reactor – II (EBR-II). However, this approach relies upon reactor calculations for input quantities of SNM and involves destructive analysis based sampling that does not meet the timeliness requirements of the International Atomic Energy Agency. Therefore, it is not appropriate for achieving safeguards of facilities operating in non-nuclear weapons states. Thus an alternative method of safeguarding SNM is required for pyroprocessing

In this section, pyroprocessing's history, key operations, and potential safeguards approaches are described. The description of key operations focuses on aspects of

pyroprocessing that inhibit the application of MC&A as a reliable safeguards approach. Proposed alternatives to MC&A for safeguarding pyroprocessing are discussed to provide the motivation and context of this work.

1.1 History

Until the 1980s, very little research had been done on the electrorefining of SNF. In the mid-1950s, Knolls Atomic Power Laboratory used electrorefining to decontaminate irradiated uranium [2]. At Los Alamos National Laboratory, in the 1960s, plutonium was successfully electrorefined from used fuel from the Los Alamos Molten Plutonium Reactor Experiment [3]. In 1984 research began at Argonne National Laboratory (ANL) on the Integral Fast Reactor (IFR) [4]. Accompanying the IFR was a pyrochemical process – pyroprocessing – that reprocessed fuel from the IFR.

Before ANL's work, uranium and plutonium had not been simultaneously electrorefined. The work at ANL laid the groundwork for the demonstration of the IFR. At INL, EBR-II would serve as the test bed for the IFR developmental program along with the Fuel Conditioning Facility (FCF). The designed pyrochemical process would be used to separate used fuel, fabricate uranium-plutonium-zirconium fuel and process high-level waste. However, in 1994 EBR-II was shutdown marking the end of U.S. IFR program [5]. Notwithstanding, the FCF could still be used to process EBR-II used fuel to make it suitable for permanent disposal. Demonstration of pyroprocessing to treat the used EBR-II fuel was completed from 1996 to 1999 at INL in the FCF and Hot Fuel Examination Facility (HFEF). In 2000, treatment of EBR-II fuel resumed in FCF and continues to this day.

In 2002, the Advanced Fuel Cycle Initiative (AFCI) funded continuing research and development of pyroprocessing. Under AFCI, the process was expanded to include spent oxide fuel reduction expanding pyroprocessing capabilities beyond metal fuel processing.

In addition to the work in the US, Japan's Central Research Institute of Electric Power Institute (CRIEPI) and the Korea Atomic Energy Research Institute (KAERI) are actively researching pyroprocessing. KAERI especially has been aggressively pursuing pyroprocessing technologies. In late 2011, KAERI finished construction on a 10t/yr pyroprocessing facility named PRIDE (PyRoprocess integrated Inactive DEmonstration) facility which does not process SNF, rather a surrogate uranium based material [6]. While there are other countries researching pyroprocessing, these two countries are of particular interest because they do not currently possess nuclear weapons. For these two countries, or any other non-nuclear weapons states, the possibility of pyroprocessing being misused for military purposes needs to be examined. Providing an assurance of nuclear safeguards would be an important prerequisite for any commercial development of pyroprocessing technology.

1.2 Description of Pyroprocessing

INL has developed pyroprocessing on an engineering-scale at the FCF. This facility is the ideal candidate for the safeguards analysis of pyroprocessing because of its well-documented operation, the extensive nature of available data and its size. As presently constituted at INL's FCF, pyroprocessing is a batch process. Due to the high radioactivity of SNF, the process is setup in an argon filled hot-cell and remotely maintained and controlled.

The material moves from one unit of operation to the next in discrete movements. A simplified flow chart of pyroprocessing of metallic spent fuel is shown in Figure 1.1. A more detailed description of the entire process is available in other publications [7, pp. 28-32, 8, pp. 3-6]. Notably, oxide spent fuel can be processed if it is first electrochemically reduced to metallic form. This adds only one to three additional steps to the process given in Figure 1.1.

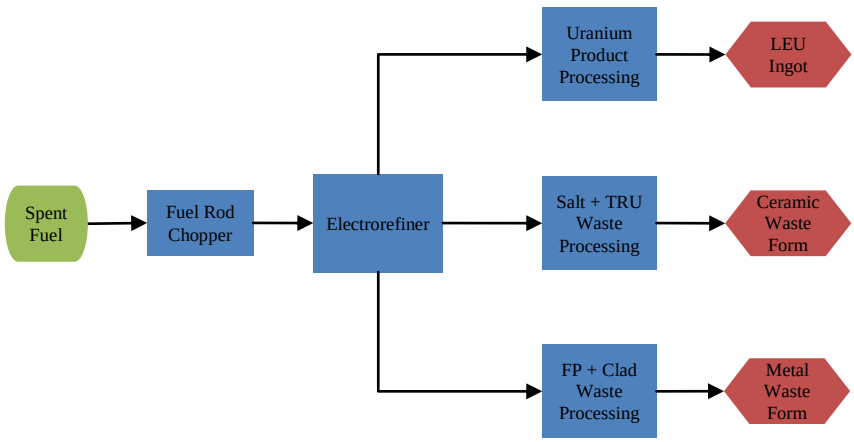

Figure 1.1 Simplified Flowchart of Pyroprocessing

Initially, the SNF rods are chopped into small quarter-inch pellets. These pellets are loaded into perforated baskets which serve as the anode in the electrorefiner (ER). Up until the ER, all of the feed material flows in one line. The ER partitions SNF into three phases: anode baskets, electrolyte and cathode deposits. Once the anode baskets have been loaded into the ER, a current is applied. Uranium, other actinides and the more active fission products (FP) in SNF are oxidized and transported into the electrolyte. Of the species oxidized, uranium is the least stable in the electrolyte and deposits on the cathode. The

uranium product is processed into an ingot of low-enriched uranium (LEU). The transuranics (TRU) and fission products remaining in the salt are processed into a ceramic waste form. The fission products remaining in the anode baskets are processed along with the fuel cladding into a metal waste form. Both waste forms are considered high-level waste (HLW).

Several aspects of this process design provide challenges for the use MC&A. First the feed material is not homogeneous. The isotopic composition of SNF varies spatially which results in each chopped fuel rod segment having a different composition. The amount of each nuclide fed to the process is predicted using ORIGEN calculations and adjusted based on random sampling which introduces uncertainty and a time delay. Second, there is a large amount of material hold-up in the ER, which further complicates the task of mass tracking.

1.2.1 Electrorefiner

Pyroprocessing at INL's FCF consists of two parallel lines, one for EBR-II's driver fuel and the other for EBR-II's blanket fuel, each with its own ER, the Mark-IV and Mark-V respectively. The research presented in this thesis focuses on the Mark-IV ER configuration. A representation of the Mark-IV electrorefiner is found in Figure 1.2. The Mark-IV uses four rectangular stainless steel fuel baskets arranged in a cruciform geometry as the anode. The anode is loaded into a molten eutectic mixture of 59 mol% lithium chloride (LiCl) and 41 mol% potassium chloride (KCl) which serves as the electrolyte. Beneath the electrolyte is a molten cadmium pool. The cathode is a solid-steel rod upon which uranium deposits as

dendrites. The electrorefiner operates at 500°C. During operation the LiCl-KCl mixture is stirred by the rotation of the electrodes. The cadmium pool is mixed by a stirrer.

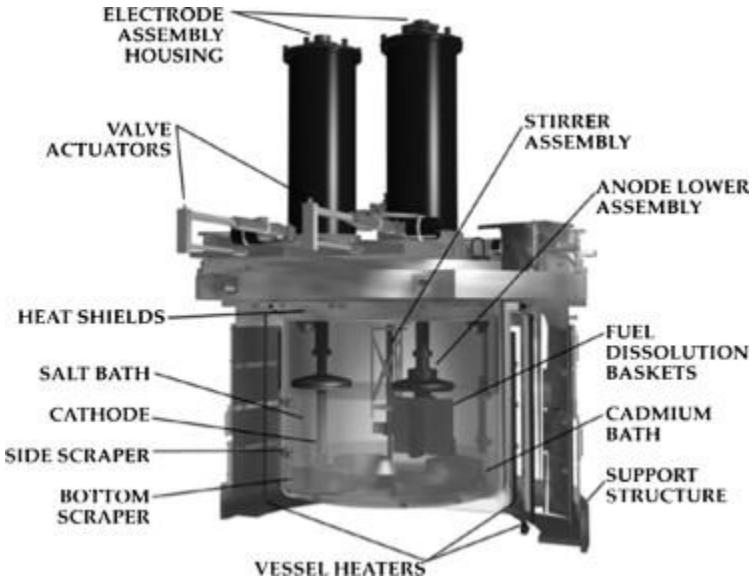

Figure 1.2 Mark-IV Electrorefiner[9]

As mentioned previously, the feed material for the Mark-IV is EBR-II's driver fuel. Li and Simpson[10] performed a study in which the typical composition of SNF in the anode baskets was determined. While composition varies from batch to batch, Table 1.1 gives an idea of the more prevalent species in the system.

Table 1.1 EBR-II Spent Fuel Composition [10]

Element	Weight (g)	Wt%
Uranium	8070	80.6
Zirconium	1080	10.8
Sodium	216.0	2.16
Neodynium	93.10	0.930
Cesium	77.30	0.773
Molybdenum	77.20	0.771
Cerium	54.20	0.542
Plutonium	41.40	0.413
Ruthenium	40.70	0.407

1.3 Safeguards

Safeguards are a collection of verification and inspection methods used to ensure the peaceful use of nuclear materials. The main objective of safeguards according to the International Atomic Energy Agency (IAEA) is "the timely detection of diversion of significant quantities of nuclear material from peaceful nuclear activities to the manufacture of nuclear weapons or of other nuclear explosive devices or for purposes unknown, and deterrence of such diversion by the risk of early detection" [11, p. 13]. Safeguards are applied to facilities that handle nuclear material. These include enrichment plants, fuel fabrication plants, nuclear reactors and reprocessing plants among others. Because pyroprocessing is considered reprocessing technology, safeguards are required for the process.

Pyroprocessing holds an advantage in proliferation resistance over the traditional aqueous based PUREX (Plutonium – URanium EXtraction) process. In the PUREX process, pure plutonium is isolated from other actinides and fission products. Subsequently, uranium and plutonium are blended back together in the process for use as mixed-oxide fuel (MOX).

Alternatively, pyroprocessing selectively removes uranium from SNF and plutonium is left in a mix of actinides and active fission products or co-extracted with uranium. However, no fuel separation technology can be assumed immune to being misused for diversion of SNM.

1.3.1 Traditional Safeguards

Traditionally, the tracking of materials is accomplished by MC&A. With PUREX, this is more readily accomplished. At the beginning of the process, SNF is completely dissolved in a dissolution tank commonly referred to as the "accountability tank." This tank provides a homogeneous sample from which the composition of the feed can be determined. Because PUREX is a continuous process, the flow of this material can be tracked through the system using flow rates. Thus by performing material balances on the process an expected product inventory can be calculated and used to verify that the actual inventory is within a tolerable amount of error. MC&A is a proven method for safeguarding the PUREX process, as a case in point being the Rokkasho Reprocessing Plant in Japan.

The tolerable amount of error, as determined by the IAEA is one significant quantity (SQ) or less over a material balance period [11, p. 25]. A material balance period is the time between two consecutive physical inventory measurements. A SQ is "the approximate amount of nuclear material for which the possibility of manufacturing a nuclear explosive device cannot be excluded" [11, p. 23]. These amounts are shown in Table 1.2.

Table 1.2 Significant quantities for SNM as determined by the IAEA [11]

Material	Amount
Direct Use Nuclear Material	
Pu (containing less than 80% ^{238}Pu)	8 kg
^{233}U	8 kg
Highly Enriched Uranium (HEU) – ^{235}U ≥ 20%	25 kg*
Indirect Use Nuclear Material	
Low-Enriched Uranium (LEU) - ^{235}U < 20%,	75 kg*
Natural Uranium	10 t
Depleted Uranium	20 t
Thorium	20 t
*Amount refers to mass of the ^{235}U isotope	

Early analyses of the application of traditional safeguards to pyroprocessing demonstrate an unacceptably high level of inventory uncertainty [7, 12]. Uncertainty in the inventory of SNM is introduced by the feed material. Because pyroprocess has no "accountability tank" or any other homogeneous mixture before the process, the feed inventory is approximated using burn-up calculations. These calculations are verified or corrected using destructive analysis (DA) of random spent fuel rod samples which can create a lag-time of months.

In addition to the challenge of characterizing the feed SNF, the material needs to be tracked in the system. Non-destructive assay (NDA) techniques could provide some insight into the flow of material, but "have an uncertain level of several percent" [7, p. 34]. Also complicating the use of NDA is the high radiation environment. Additionally, the large amount of holdup of plutonium in the ER adds a significant level of uncertainty. Simpson [12] reports that "realistic sampling and analytical chemistry error can result in discrepancies

near the 8 kg significant quantity for Pu based on a realistic total inventory in an industrial-scale electrorefiner."

1.3.2 Pyroprocessing Safeguards

Several options and methods have been proposed for pyroprocessing to either compensate for the shortfall of traditional safeguards or alter the approach of safeguards to take advantage of some features of pyroprocessing. Methods and approaches are still being developed and designed. INL is currently developing an acceptable safeguards approach for pyroprocessing using the "FCF as a scientific and experimental baseline" [1, p. 1]. Similarly, South Korea has been researching possible safeguards methods [13]. This section reviews the specific tools and methods being developed for safeguarding pyroprocessing.

1.3.2.1 Neutron Balance and Curium Accounting

Part of many of the proposed options for safeguarding is a neutron balance [14, pp. 30-31]. This involves a total neutron measurement of each pin of SNF introduced into the process, the electrorefiner, the metal waste form, the ceramic waste form and the uranium product. It would also incorporate process monitoring of the electrorefiner [14, p. 30].

The bulk of the neutrons in SNF are attributed to curium. The plutonium-to-curium ratio (PCR) of SNF can be determined using DA. If that ratio is assumed to be constant throughout the process, the amount of plutonium can be determined from neutron count. However, it is not certain that "[curium] would completely transfer with [plutonium] in a pyroprocessing facility" [1, p. 3]. INL performed curium measurements which demonstrated

the difficulty of tracking plutonium using curium. In the experiments, there was not a significant accumulation of curium in salt to be detected using DA. However, this work was performed EBR-II, a fast reactor, spent fuel which has low curium-244 content. Likewise, South Korea is researching the applicability of Laser Induced Breakdown Spectroscopy (LIBS) and high-resolution gamma-ray spectroscopy coupled with FRAM analysis code for the real-time monitoring of the PCR [13].

1.3.2.2 Electrorefiner Assay

This technique is essentially a mass balance on the electrorefiner. This requires a series of assays on all streams entering and leaving the electrorefiner over multiple batches. The method "relies on elaborate analyses that would certainly impact operations and cause delays between processing steps" [14]. Additionally, the assumption of a constant PCR is made which, as discussed, is not a certainty in pyroprocessing. However, process monitoring could be used to confirm the validity of the assumption.

1.3.2.3 Homogenized Input

Another suggested method is to homogenize the input by producing a molten solution of the chopped fuel elements that is well-mixed [14]. This would allow for an accurate assessment of plutonium feed inventory and the PCR. The plutonium would then be tracked through the system using neutron counting and the PCR. Again, DA is required to verify that the PCR is constant throughout the process and, thereby, the predicted plutonium content.

This method would provide the means for MC&A to be accurately applied to pyroprocessing. However, this is disruptive and would require modifications to the pyroprocess.

1.3.2.4 Digital Cloud Chamber and Inverse Spectroscopy Algorithm

INL has developed a method by which non-homogeneous samples can be characterized [1]. It uses a digital cloud chamber (DCC) to record the pathways of gamma rays and neutrons. Using the data from the DCC in conjunction with the inverse spectroscopy algorithm, the energy and originating location of the incident radiation can be determined. This tool could be used for quantifying plutonium in SNF or other containers in the pyroprocess [15]. It should be noted that this detection method requires a long measurement time making it better suited for evaluating feed and product inventory rather than intermediary products in the pyroprocess.

1.3.2.5 Goals Driven Safeguards

One of the proposed alternatives to traditional safeguards is Goal Driven Safeguards (GDS) as described by Wigeland et al. [7]. This approach takes advantage of the batch nature of pyroprocessing. The material is moved between process units in containers. Each container would be weighed and numbered marking the creation of an "item." Each item would be tracked through the system. The movement of the item would be recorded and monitored. In pyroprocessing under normal operation, there is a unique set of motions between each unit of operation. If a movement was recorded outside of the normal operating paths, it would signify abnormal operations and the possibility of diversion.

The location of the process in a shielded hot cell is also advantageous. The hot cell has a limited number of portals. These portals could be monitored using NDA methods to ensure that products leaving the cells are consistent with their declaration. Lack of accuracy in NDA methods would be compensated by the item and motion tracking within the cell.

1.3.2.6 Signature-Based Safeguards

Signature-Based Safeguards [12] build upon the principles of Goals-Driven Safeguards and adds a process model to identify measurable indicators (signatures) of diversion of SNM. These include, but are not limited to temperature, density, voltages, current, etc. The process model would simulate potential diversion scenarios to identify combinations of measurements, movements and other conditions that are indicative of diversion. This model would run in real-time in parallel to the actual process. It would use the sensor readings to determine if diversion of SNM is occurring and sound an alarm if the conditions matched that of a diversion scenario. In addition to Signature-Based safeguards, other methods of incorporating a process model to support and compliment MC&A have been proposed [16].

In order to accomplish Signature-Based Safeguards "chemically and physically correct representations of each unit operation should be built" [12]. Additionally, many of the safeguards methods mentioned above require process monitoring. The ER is most important and complex unit of operation because it partitions the SNF. It would be the ideal location for potential proliferators to alter the flow of material. A better understanding of electrorefiner can be accomplished through simulating its performance. A model of the ER would help in determining the validity of a constant PCR and in developing Signature Based Safeguards. In

both cases, the flow of plutonium is of specific interest. Thus, the conditions under which plutonium could be removed from the salt and co-deposited with uranium is of particular interest.

2 Theory

In order to accomplish the goals of Signature-Based Safeguards and other pyroprocessing safeguard methods, a certain level of understanding of electrochemical theory is required. An electrochemical cell, such as the electrorefiner, combines the physical phenomena of reaction kinetics, thermodynamics and mass-transport. Most models of the electrorefining process are based upon the electrochemical theory discussed in this section.

2.1 Electrochemical Cell

An electrochemical cell consists of four main components: a power supply, an anode, a cathode and an electrolyte. The power supply drives the reaction. Material is oxidized at the anode and reduced at the cathode. The electrolyte serves as conducting medium to allow the flow of ions and electrons in the cell. A representation of Mark-IV electrochemical cell is shown in Figure 2.1. In the case of the Mark-IV, SNF is oxidized from the anode and uranium is reduced at cathode while other elements in SNF remain in the salt or the anode baskets under normal operating conditions. EBR-II SNF is metallic resulting in a reaction of oxidizing a metal species at the anode and the reduction of a metal ion at cathode. These reactions are shown in (2.1).

Anode: $$j \leftrightarrow j^{n+} + n \cdot e^{-} \quad (2.1a)$$

Cathode: $$j^{n+} + n \cdot e^{-} \leftrightarrow j \quad (2.1b)$$

In these equations, j represents any species in SNF, n is the number electrons exchanged and e^{-} represents an electron. At any time, multiple species can be reacting at either electrode.

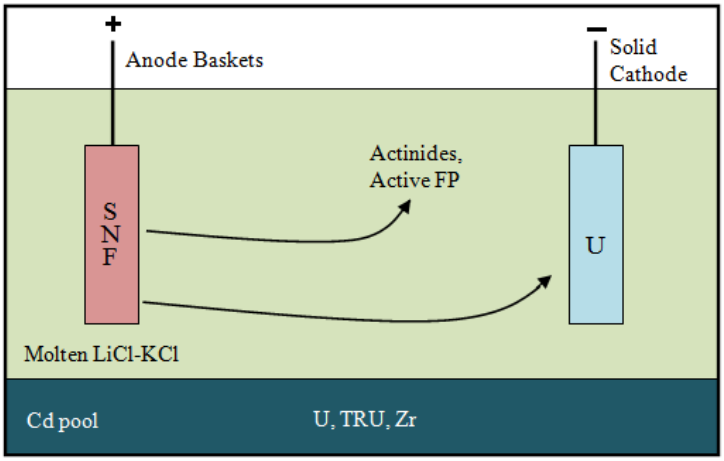

Figure 2.1 Representation of the Mark–IV electrochemical cell

2.2 Potential

The potential of an electrode is composed of two parts: the equilibrium potential, E_{eq}, and overpotential, η [17].

$$E = E_{eq,j} + \eta_j \quad (2.2)$$

The equilibrium potential is given by the Nernst equation [18, p. 19]:

$$E_{eq,j} = E_j^o + \frac{\nu \cdot R \cdot T}{n_j \cdot F} ln\left(\frac{a_{j^{n+}}}{a_j}\right) \tag{2.3}$$

where E_j^o represents the standard reduction potential of species j, ν is the stoichiometric coefficient (+1 for oxidation and -1 for reduction), R is the universal gas constant, T is the temperature of the electrochemical cell, F is Faraday's constant, and a represents the activity of a species. The activity of the reduced metal, a_j, is taken to be unity. The activity of the oxidized species is related to the concentration, C, by the activity coefficient, γ, and is relative to a standard concentration, C^o, as shown[18, p. 19].

$$a_{j^{n+}} = \frac{\gamma_{j^{n+}} \cdot C_{j^{n+}}}{C^o} \tag{2.4}$$

The standard concentration is commonly taken to be 1 mol/L [19].

The overpotential can be split into two terms: surface (η_s) and concentration (η_c) overpotential [17].

$$\eta_j = \eta_{c,j} + \eta_{s,j} \tag{2.5}$$

The concentration overpotential is created by mass-transfer limitation near the electrode. This limitation creates a thin layer next to each electrode, commonly referred to as the diffusion boundary layer, in which a concentration difference exists between the bulk of the electrolyte and the surface of the electrode. A certain amount of potential is consumed to drive species

through the diffusion layer and is calculated by the following equation [17]:

$$\eta_c = \frac{R \cdot T}{n_j \cdot F} ln\left(\frac{C_{j^{n+}}^{S}}{C_{j^{n+}}}\right) \tag{2.6}$$

where $C_{j^{n+}}^{S}$ represents the mole fraction of the ion of species j at the electrode surface. The surface overpotential is determined using the Butler-Volmer equation which is discussed later.

The potential of each electrode determines which species are oxidized or reduced. For example, in order for a species to reduce at the cathode, the species' equilibrium potential needs to be less negative than the cathode's potential. Electrode potentials are measured in reference to another electrode. The reference electrodes used in the Mark-IV electrorefiner are silver/silver-chloride (Ag/AgCl) electrodes [20]. By observing the standard reduction potentials of the most prevalent species in EBR-II SNF (see Table 1.1), it can be determined at a standard concentration value which species will remain in the anode, be oxidized and partitioned into the salt or reduced at the cathode. Values for the standard reduction potentials at 500 °C are displayed in Table 2.1. The values are listed in descending order from most noble to least noble. The shading color corresponds to color scheme in Figure 2.1. The more active species will oxidize into the salt phase. Uranium is the least stable in the salt phase and reduces onto the cathode.

Table 2.1 Standard Reduction Potential of Species in Table 1.1 vs. Ag/AgCl Reference Electrode at 500 °C [8]

Element	E^o (V) vs. Ag/AgCl	Phase
Ruthenium	0.526*	Anode
Molybdenum	0.119*	
Zirconium	-1.088*	
Uranium	-1.248	Cathode
Plutonium	-1.555	Salt (Electrolyte)
Cerium	-2.026	
Neodymium	-2.358	
Sodium	-2.5*	
Cesium[1]	---	

*At 450 °C, [1] Position in table determined by free energy of formation of its chloride in comparison to others **[8, p. 72]**

2.3 Current

The current determines the rate of reaction. The cell current is a measure of the total net reaction rate of all species in the cell. A reliable expression for cell current is central to determining flow of material between phases in the electrorefiner. Of particular interest is the reaction occurring at the cathode for safeguard and product quality purposes.

To begin the development of an expression for cell current, the current and reaction rate need to be linked. Faraday's constant, F, relates the current of a species, I_j, to the reaction rate of a species, r_j [18, p. 10]:

$$I_j = F \cdot n_j \cdot A \cdot r_j \tag{2.7}$$

where A is the surface area of the electrode. Assuming the reactions in (2.1) to be single-step

the reaction rate is given by [18, p. 17]:

$$r_j = k_{f,j} \cdot C_{j^{n+}}^{s} - k_{r,j} \cdot C_j^{s} \tag{2.8}$$

where C_j and $C_{j^{n+}}$ are respectively the concentrations of the reduced and oxidized species j, and $k_{f,j}$ and $k_{r,j}$ are the forward and reverse rate constants for species j. (2.8) refers to the reduction reaction as the forward reaction and the oxidation reaction as the reverse. In electrochemistry, the rate constants, k, have an Arrhenius dependence on potential[18, pp. 20-21]:

$$k_{f,j} = k_j^o \cdot exp\left(-\frac{\alpha_j \cdot n_j \cdot F}{R \cdot T} \cdot E - E_{eq,j}^o\right) \tag{2.9}$$

$$k_{r,j} = k_j^o \cdot exp\left(\frac{(1-\alpha_j) \cdot n_j \cdot F}{R \cdot T} \cdot E - E_{eq,j}^o\right) \tag{2.10}$$

where k_j^o is the standard rate constant taken at a standard concentrations for the oxidized and reduced species. This standard concentration is commonly taken to be 1 mol/L [19]. α_j is the transfer coefficient. $E_{eq,j}^o$ is equilibrium condition at which k^o is determined. If the concentration of the oxidized species is at the standard value of 1 mol/L then by using (2.3) and (2.4) then E_{eq}^o is given by the following equation.

$$E_{eq,j}^o = E_j^o + \frac{R \cdot T}{n_j \cdot F} ln\left(\gamma_{j^{n+}}\right) \tag{2.11}$$

where $C_{j^{n+}}^o$ is the standard concentration at which k_j^o is determined. By combining (2.7), (2.8), (2.9) and (2.10), the basis for the Butler-Volmer (B-V) equation is formed.

$$I_j = n_j \cdot F \cdot k_j^o \cdot A \cdot \left(e^{-\frac{\alpha_j \cdot n_j \cdot F}{R \cdot T} \cdot E - E_{eq,j}^o} \cdot C_{j^{n+}}^{s} - e^{\frac{(1-\alpha_j) \cdot n_j \cdot F}{R \cdot T} \cdot E - E_{eq,j}^o} \cdot C_j^{s}\right) \tag{2.12}$$

The leading term in (2.12) is commonly represented as the standard exchange current, as shown below.

$$I_{o,j}^{o} = n_j \cdot F \cdot k_j^{o} \cdot A \tag{2.13}$$

Often the area term is divided out of (2.13) to remove the area dependence resulting in the standard exchange current density, $i_{o,j}^{o}$.

At this point, a slight diversion will be made to discuss the current under equilibrium conditions. At equilibrium, the net current is zero and the bulk concentration is equivalent to the surface concentration. Using (2.12), this results in the following equation.

$$I_{o,j}^{o} \cdot e^{-\frac{\alpha_j \cdot n_j \cdot F}{R \cdot T} \cdot E - E_{eq,j}^{o}} \cdot C_{j^{n+}} = I_{o,j}^{o} \cdot e^{\frac{(1-\alpha_j) \cdot n_j \cdot F}{R \cdot T} \cdot E - E_{eq,j}^{o}} \cdot C_j \tag{2.14}$$

The current at equilibrium is referred to as the exchange current. Thus, taking the B-V equation at any arbitrary equilibrium condition, an expression for the exchange current can be developed. The general expression for the exchange current is given below [18, p. 25].

$$I_{o,j} = I_{o,j}^{o} \cdot C_{j^{n+}}^{(1-\alpha)} \cdot C_j^{\alpha} \tag{2.15}$$

However, the inclusion of a reduced species concentration term in exchange current assumes a product in solution which is not case in the ER. Specifically for the Mark-IV ER, the exchange current is derived by combining (2.3), (2.4), (2.11) and the left-hand side of (2.14) and assuming a solid product with an activity of unity.

$$I_{o,j} = I_{o,j}^{o} \cdot C_{j^{n+}}^{(1-\alpha)} \cdot {C_{j^{n+}}^{o}}^{\alpha} \tag{2.16}$$

Returning to the derivation of an expression for the cell current, the B-V equation can become more generalized by utilizing an expression developed from the combination of (2.3) and (2.11)

$$E_{eq,j} \; - \; E^{o}_{eq,j} = \frac{R \cdot T}{n_j \cdot F} ln\left(\frac{C_{j^{n+}}}{C^{o}_{j^{n+}}}\right) \tag{2.17}$$

(2.17) used with (2.2) and (2.12) results in the B-V equation being generalized to any equilibrium condition as opposed to a standard condition.

$$I_j = I_{o,j} \cdot \left(\frac{C^{s}_{j^{n+}}}{C_{j^{n+}}} \cdot e^{-\frac{\alpha_j \cdot n_j \cdot F}{R \cdot T} \cdot \eta_j} - \frac{C^{s}_{j}}{C_j} \cdot e^{\frac{(1-\alpha_j) \cdot n_j \cdot F}{R \cdot T} \cdot \eta_j}\right) \tag{2.18}$$

Specifically applying (2.18) to the Mark-IV ER, it becomes (2.19).

$$I_j = I_{o,j} \cdot \left(\frac{C^{s}_{j^{n+}}}{C_{j^{n+}}} \cdot e^{-\frac{\alpha_j \cdot n_j \cdot F}{R \cdot T} \cdot \eta_j} - e^{\frac{(1-\alpha_j) \cdot n_j \cdot F}{R \cdot T} \cdot \eta_j}\right) \tag{2.19}$$

The ratio of the surface and bulk concentrations of the reduced metal cancels out because the activity of the metal is one. The generalized B-V equation provides a means whereby the current for each species can be determined. If there is only one species depositing on the cathode, then the B-V equation evaluated at the cathode will yield the cell current.

Thus far, the case of a single species has only been considered. In the case that there is more than one reaction occurring at the cathode, the cell current is the sum of the current of all the species actively reacting [21, p. 60].

$$I_{cell} = \sum I_j \tag{2.20}$$

Under galvanostatic operation, a secondary reaction begins to occur when the primary reactant is unable to meet the requested cell current due to mass transfer limitations.

In an ER, the electrolyte is well mixed. However, there is thin layer next to the electrode through which reacting species need to diffuse. The rate of diffusion can be determined two ways. One possible method is to solve for molar flux, N_j, using the transport equation in the diffusion layer [22].

$$N_j = -D_j \cdot \nabla^2 C_j - \nabla\left[\frac{n_j \cdot F \cdot D_j \cdot \nabla E}{R \cdot T}\right] \tag{2.21}$$

where D_j is the diffusion coefficient. The other method is to use a mass-transfer coefficient, h_j, which encompasses all of the dynamics accounted for in the transport equation which is accomplished using the following equation [8, p. 20].

$$I_j = n_j \cdot F \cdot N_j = n_j \cdot F \cdot h_j \cdot A \cdot \left(C_{j^{n+}} - C^s_{j^{n+}}\right) \tag{2.22}$$

The limiting current occurs at largest concentration difference. This occurs when the surface concentration is zero. If the limiting current for the primary species is less than the requested cell current, another species needs to deposit on the cathode to meet the requested value.

3 Models

Three models were available for investigation of signatures and methods to be used in safeguarding pyroprocessing. The first model was developed by Robert Hoover at the University of Idaho (UI) [8]. The second was Enhanced REFIN with Anodic Dissolution (ERAD) which is an adaptation of the REFIN code developed by B. G. Park at Seoul National University in Korea [22]. The last model was developed by Jun Li at the University of North Carolina (UNC) [23]. This section provides an overview of each model and the rational for selecting a model to use in investigating potential safeguard signatures.

3.1 UI Model

This model was developed as part of a joint project with UI, INL, KAERI and Seoul National University. The model provides operation voltages and currents along with composition of the anode, salt and cathode. Also, the model allows for the user to specify the applied current, initial composition of the anode, salt and cathode. This code used the B-V equation to account for kinetics and the mass-transfer coefficient for mass transport in the diffusion layer. The exchange current density was empirically fit to match data from the Mark-IV electrorefiner and assumed to be constant with respect to concentration and the same for each species. The model only accounts for the reaction and transport of uranium, zirconium and plutonium in the Mark-IV and excludes the reduction of plutonium at the cathode.

3.2 ERAD

ERAD introduces a number of additions and alterations to REFIN to account for different physical phenomena and to improve the speed and convergence of the solutions. The general approach of the model is similar to the Hoover model but accounts for more physical processes and is more versatile. One difference is that before the diffusion layer on the anode, there is a crud layer that builds up with time that the nuclides have to diffuse through. Another difference is the mass-transfer treatment. ERAD solves the mass transport equation for ionic solutions, discussed in detail elsewhere [22]. Also, ERAD accounts for concentration dependence of exchange current density. However, neither ERAD nor the UI model has an experimentally verified value for the standard exchange current density for any

of the species. ERAD can account for up to 10 radionuclides. In a comparison to experimental data, ERAD demonstrated good agreement in electrode potential, but over-predicted plutonium transport and under-predicted uranium transport. In addition, zirconium dissolution did not agree well with the experimental data [24].

3.3 UNC Model

The previous two models are both considered one-dimensional. This model is three-dimensional. The model uses ANSYS-CFX to generate a three-dimensional computational fluid dynamics model. Using B-V equation to set the boundary conditions, the model solves the transport equation to obtain species concentration distribution. The UNC model is able to account for potential gradients along the electrodes; whereas, the UI model and ERAD assume a uniform potential distribution along the electrodes. Also, the UNC model can capture the current density distribution at the interface of the molten salt and cadmium pool. Thus, it is best equipped to capture the effects of the cadmium pool.

3.4 Selection

The selection of a model was based on accuracy, availability and adaptability. The UI model proved to be accurate for normal operation of the Mark-IV ER. However, because the exchange current density was empirically determined and was considered constant, it can't be extended over large concentration ranges. This is required for the investigation of signatures because diversion of SNM is considered an off-normal operation and could occur at various concentration values. Additionally, the UI model does not account for plutonium

deposition at the cathode. The UNC model is the most thorough of the models. However, for an initial investigation of signatures, this model is overly advanced. The UNC model would be useful in a more advanced investigation of signatures and may be used in future work, but adds complexity which may not be necessary in this project. ERAD demonstrated to be versatile because of its roots in fundamental electrochemistry, but is not overly complicated. It too has been benchmarked against experimental data demonstrating accuracy particular in regards to electrode potentials. Thus, ERAD was selected for an initial look at the dynamics of an ER in off-normal operating condition for the purpose of identifying signatures.

4 Diversion

As discussed previously the goal of safeguards is the timely detection of diverted SNM. In general, the diversion of SNM can be accomplished in two ways: abrupt and protracted diversion [11, p. 21]. Abrupt diversion is the diversion of one SQ or more of SNM from a process in less than one material balance period. Protracted diversion is the diversion of one SQ or more of SNM over one or more material balance periods. Protracted diversion can be easier to mask than abrupt diversion. For this purpose, this work investigates the case of protracted diversion of SNM in the ER.

One possible method of protracted diversion in the ER is for small amounts of plutonium to co-deposit with uranium at the cathode. Co-deposition of uranium and plutonium can be accomplished by using a liquid cadmium cathode (LCC). This is explained by Vaden to be due to the fact that the activity coefficient of plutonium in cadmium is

significantly lower than that of uranium [25]. However, the exchange of the standard solid steel cathode for a LCC would require a movement outside of the standard operating paths.

A more difficult diversion scenario to detect would be one that uses the standard solid cathode. An experiment performed at ANL demonstrated the feasibility of the co-deposition of plutonium on a solid cathode when the ratio of plutonium-to-uranium (PUR) salt concentrations is sufficiently high [26]. The PUR in the salt phase of the ER rises naturally over time due to the nature and objective of electrorefining. At the anode, an impure product, SNF, is being oxidized while a relatively pure product, uranium, is depositing at the cathode. Thus the uranium being removed from the ER is more than the uranium being drawn from the SNF because of the oxidation of actinides and active fission products. In the Mark-IV ER, $CdCl_2$, which oxidizes any metal uranium in contact with salt, was occasionally added to maintain a desired concentration of uranium-chloride (UCl_3) in the salt [8]. Thus, protracted diversion could occur by suspending the addition of $CdCl_2$ and allowing UCl_3 concentration to gradually decrease. This particular diversion scenario was selected for the examination of potential signatures and the application of detection methods.

5 Plutonium-to-Uranium Ratio Study

To examine the behavior of certain measures in diversion scenario previously discussed, the ER was simulated using ERAD at varying PUR values. The ER was simulated in controlled current operation with a solid steel cathode. 12 cases were simulated each with a unique initial PUR value. The specific values for each case are displayed in Table 5.1. The operating cell current was fixed at 100 A for 38.8 hours in each case. Case 1 is considered the

"base" case which represents the concentrations of uranium and plutonium under normal Mark-IV operation. For a complete documentation of input parameters and settings, a copy of the ERAD input file (inpref) for Case 1 is found in Appendix A. The only values that changed from case to case in the input file were the concentrations of uranium and plutonium in the salt.

Additionally, the PUR study was performed at two different settings to compare the performance of a fixed and variable exchange current density (EXCD). The first setting is a concentration independent (fixed) EXCD. For the second setting, the EXCD was allowed to vary as the concentrations of uranium and plutonium were altered in the PUR study. In the second case, the standard EXCD for uranium, plutonium and zirconium was assumed to be 0.8, 1.1 and 0.8 A/cm^2 respectively.

5.1 Results

5.1.1 Constant EXCD

The following results were obtained while fixing the EXCD at 0.5 A/m^2 for uranium, plutonium and zirconium. The EXCD was not allowed vary with concentration during the simulation. The amount of plutonium depositing on the cathode was tracked during each case. In Table 5.1, the total amount of plutonium that deposited on the cathode in each case is shown. In cases 3, 5, 6 the amount of plutonium deposited is actually higher than the following case which has a higher PUR. A plot of the cumulative amount of plutonium deposited on the cathode at any time during the ER simulations for each PUR case is shown

in Figure 5.1. The measure of time used is the charge passed in megacoulombs (MC). The case number is indicated by the boxed number with a line pointing to curve to which it corresponds. Some cases are so close in their values that they overlap. In this case, it may appear that multiple case numbers are pointing to the same line, however; that is not the case, there are multiple lines on top of the other.

Table 5.1 Test matrix and plutonium deposited using a fixed EXCD of 0.5 A/m^2

Case Number	**1**	**2**	**3**	**4**	**5**	**6**
Pu-to-U ratio	0.031	0.091	0.254	1.149	2.621	4.511
U in Salt (wt%)	7.567	2.567	2.234	2.234	1.234	1.234
Pu in Salt (wt%)	0.234	0.234	0.567	2.567	3.234	5.567
Pu deposited (g)	0.00	31.4	1014.98	893.35	2631.46	2604.41
Case Number	**7**	**8**	**9**	**10**	**11**	**12**
Pu-to-U ratio	6.132	13.527	19.878	26.136	33.962	41.170
U in Salt (wt%)	1.234	0.313	0.213	0.213	0.213	0.200
Pu in Salt (wt%)	7.567	4.234	4.234	5.567	7.234	8.234
Pu deposited (g)	2597.85	5591.84	5915.57	5915.71	5916.83	5916.83

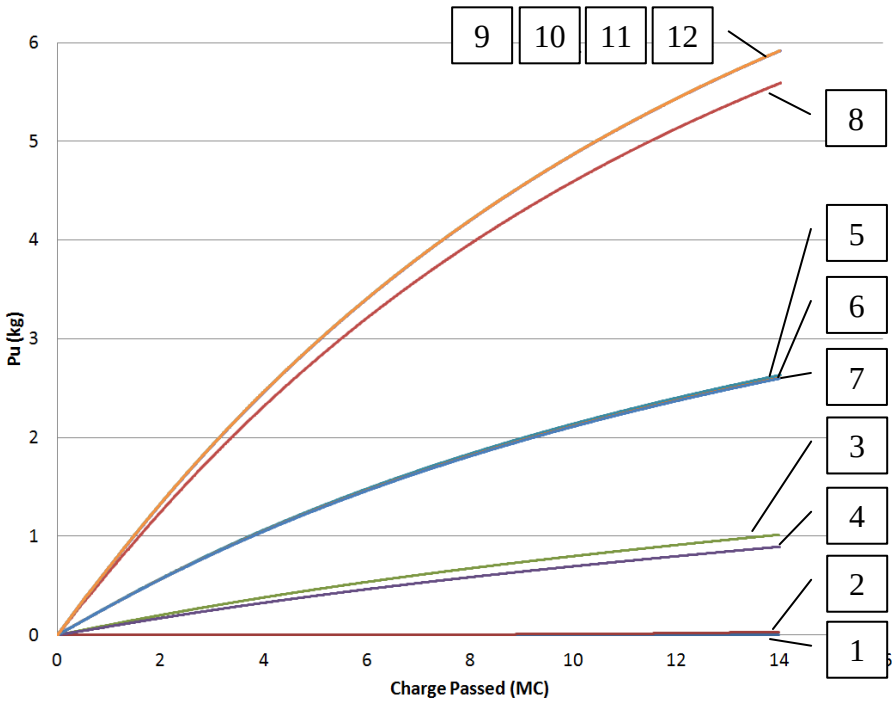

Figure 5.1 Plutonium deposited on cathode at each PUR value for a fixed EXCD

Also, included are plots of the cathode and anode potentials (see Figure 5.2 and Figure 5.3) for each PUR case. Again, numbered boxes point to the curve that corresponds to the case number. The general trend is a decreasing potential for increasing PUR values. However, this is not the case for cases 3, 5, 6 and 9, 10 which have lower potentials than the subsequent cases. The change in the anode potentials are on a smaller scale than the cathode potentials and the differences are most pronounce near the beginning of the simulation. The anode potential decrease with increasing PUR values without exception.

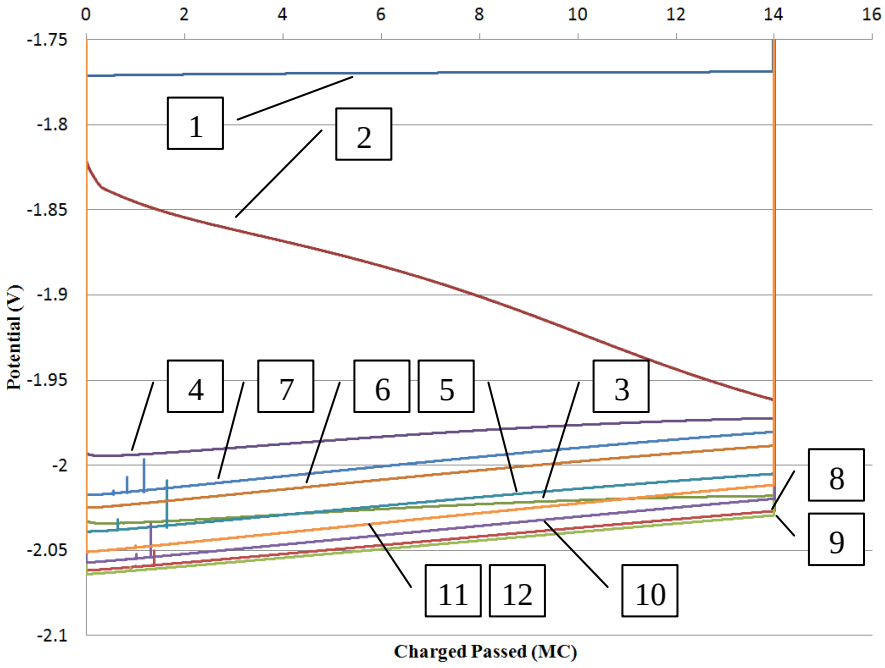

Figure 5.2 Cathode potentials at each PUR value for a fixed EXCD

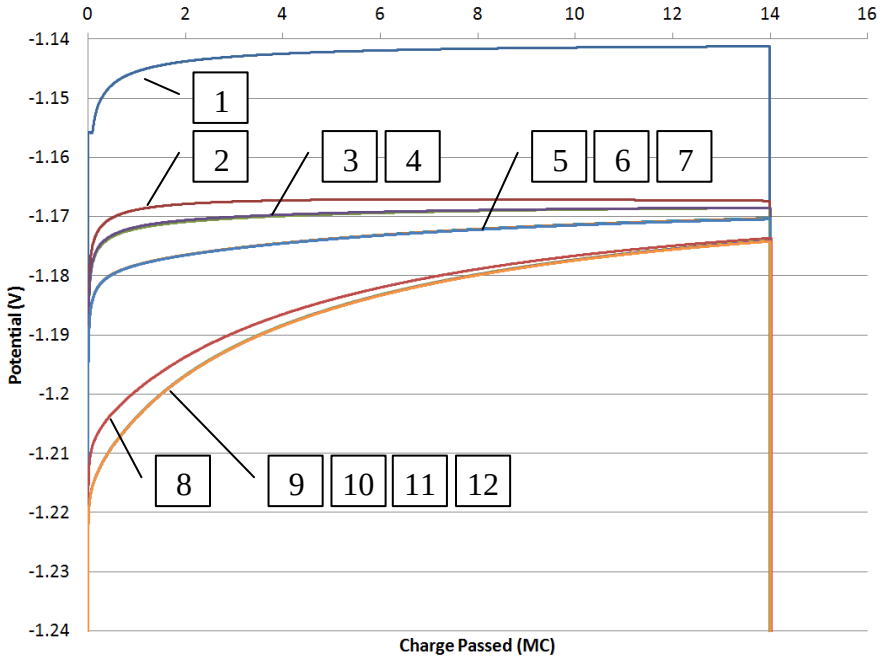

Figure 5.3 Anode potentials at each PUR value for a fixed EXCD

5.1.2 Variable EXCD

The 12 cases were simulated again allowing for variation in the EXCD due to concentration changes. The same results that were presented for the fixed EXCD setting are presented here for the variable EXCD. In Table 5.2, the total plutonium deposited in each case is reported for the setting of a variable EXCD in ERAD. Unfortunately, cases 2 and 12 were unable to converge using a variable EXCD. A comparable solution was obtained for case 2 by using a slightly perturb value of 0.235 wt% for plutonium.

Table 5.2 Amount of plutonium deposited for each case using a variable EXCD

Case Number	**1**	**2**	**3**	**4**	**5**	**6**
Pu deposited (g)	0.00	$6.77 \cdot 10^{-6}$	1044.66	995.25	2711.21	2716.26
Case Number	**7**	**8**	**9**	**10**	**11**	**12**
Pu deposited (g)	2726.61	5649.73	5969.75	5988.40	6005.08	---

Similar to the fixed EXCD setting, the plutonium deposited and cathode potentials are displayed in Figure 5.4 and Figure 5.5 respectively. However, due to differences in the ERAD versions, the simulation progression was measured by time instead of the amount of coulombs passed. Despite the difference in units, the x-axes in both settings are on the same scale. Under the variable EXCD setting, the general trends of increasing plutonium deposition and decreasing cathode potential with increasing PUR holds. The only exceptions are case 4 for plutonium deposition and cases 4, 6, 7, 10 and 11 for cathode potentials.

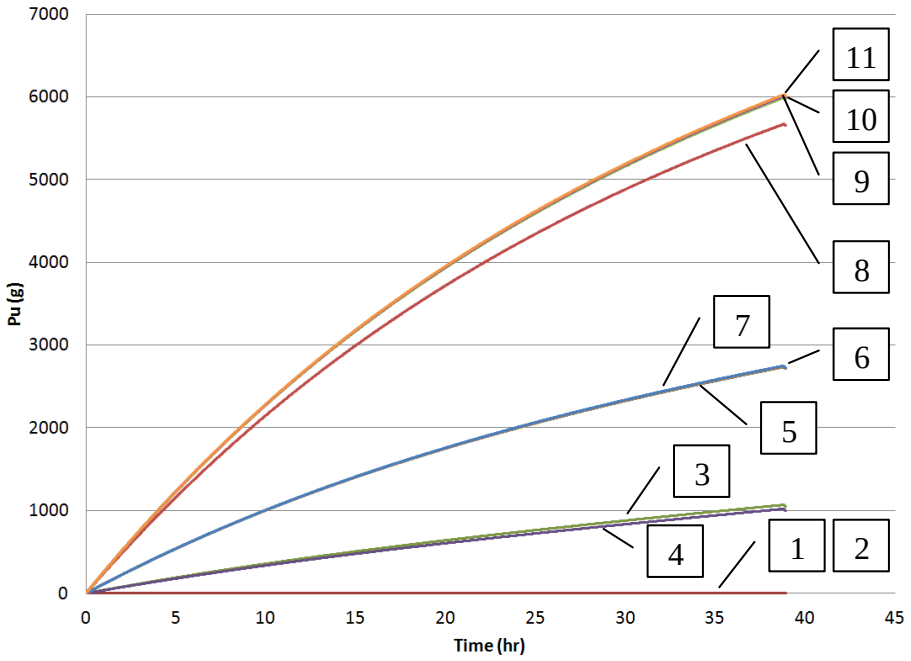

Figure 5.4 Plutonium deposited on cathode at each PUR values for a variable EXCD

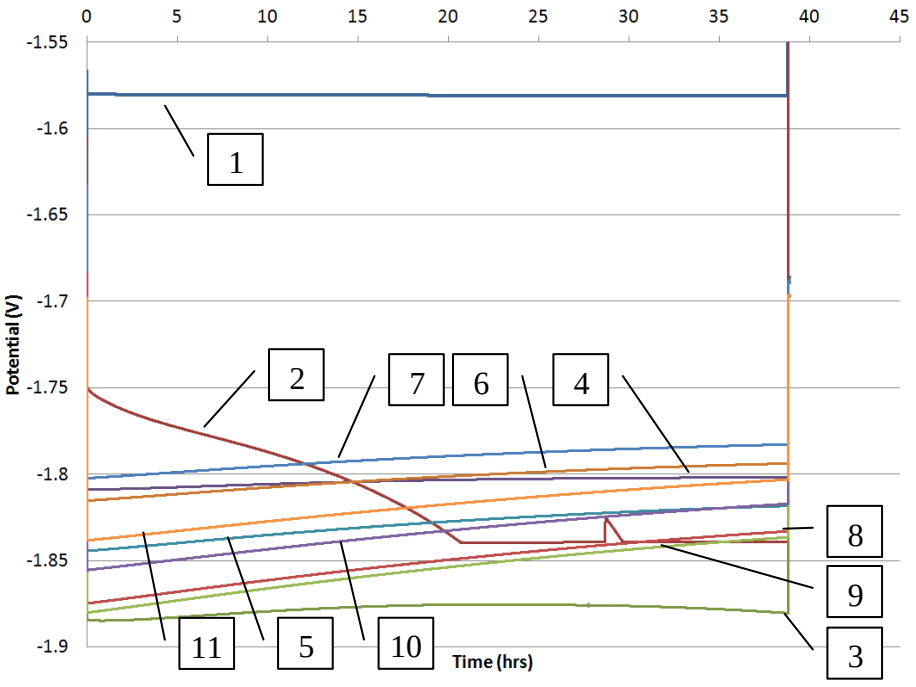

Figure 5.5 Cathode potentials at each PUR value for a variable EXCD

5.2 Discussion

In Table 5.1 and Table 5.2, the largest gains in the amount of plutonium deposited on the cathode are after cases 2, 4 and 7. In Table 5.1, it is shown that after cases 2, 4 and 7 the initial amount of uranium in the salt decreases. This indicates that the amount of uranium in the salt is a determining parameter for plutonium deposition. This is due to the principle of limiting current.

Uranium is thermodynamically favored for metal deposition over plutonium. Thus the only means whereby plutonium can deposit while uranium is present is if the concentration of uranium is low enough that its limiting current is below the requested current. In this case, the next most favorable reaction occurs. That reaction, in these studies, is plutonium reduction. The cathode potential is forced to decrease to allow the deposition of plutonium to meet the requested current for the ER cell.

This is not to say that the concentration of plutonium is irrelevant. Indeed, if the concentration of plutonium was small relative to some other species' (i.e. neptunium, zirconium) than that species could be favored to deposit over plutonium. Inspecting (2.3), shows that as the activity of a species increases, the equilibrium potential increases which means a less negative potential is required to allow deposition.

It was noted that in Table 5.1 and Table 5.2 that increasing the initial plutonium concentration, in some cases, actually reduced the total plutonium deposited on the cathode. This is due to the treatment of the cadmium pool by ERAD. At the beginning of each

simulation, ERAD performs an equilibrium calculation for each of the species between the salt and the cadmium pool. At equilibrium, the potential difference between the salt and the pool for each species is equivalent. The increase in the initial plutonium concentration in the salt causes the concentration difference of plutonium between the pool and the salt to increase which increases the potential difference for plutonium. Because the potential differences of plutonium and uranium have to match, uranium's concentration difference needs to increase as well. The concentration difference of uranium can increase by transporting less uranium into the cadmium pool. Thus, even though Table 5.1 shows that the initial amount of uranium in the salt is the same for some cases. However, that is not the case after the equilibrium calculation between the salt and the pool. In fact, the amount of uranium in the salt is slightly higher in cases 4, 6 and 7 after the equilibrium calculation resulting in less plutonium being deposited. These cases illustrate the need to understand the flow of material between the salt and cadmium phases in order to accurately simulate the ER.

5.2.1 Composition effects on signatures

By comparing Figure 5.2 and Figure 5.3, the cathode potential appears to be more sensitive to the change in uranium and plutonium salt compositions. Additionally, the anode potentials of the variable EXCD cases were lower than the anode potentials for a fixed EXCD and vice versa for cathode potentials.

Further analysis was done to examine the strength of the dependence of the anode and cathode potentials on the uranium and plutonium salt compositions. The potential of each electrode was averaged over the duration of the simulations for each case and for a fixed

EXCD of 0.5 A/m^2 and a variable EXCD. These values were plotted against the composition of uranium and plutonium in the salt (see Figure 5.6 and Figure 5.7). A linear fit was applied to the data. The values for the coefficients of the linear fit and the coefficient of determination (R^2) are displayed in Table 5.3.

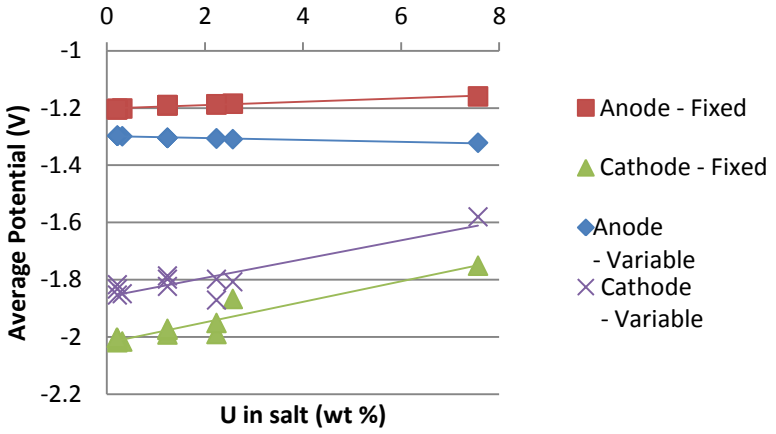

Figure 5.6 Average electrode potentials versus uranium composition in the ER salt

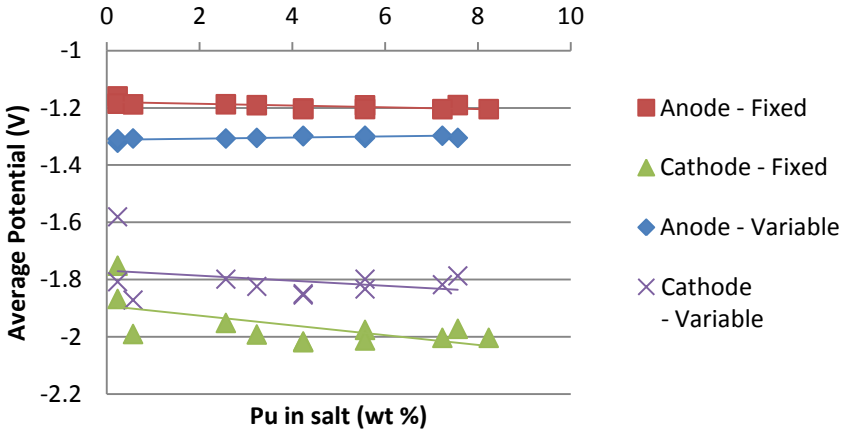

Figure 5.7 Averaged electrode potentials versus plutonium composition in the ER salt

Table 5.3 Fitting parameters for the linear equation $Y=A\cdot X+B$ for Figure 5.6 and Figure 5.7

EXCD	Salt wt% (X)	Potential (Y)	Slope (A)	Y-intercept (B)	R^2
Fixed	U	Anode	0.006	-1.202	0.937
		Cathode	0.036	-2.021	0.899
	Pu	Anode	-0.003	-1.179	0.475
		Cathode	-0.017	-1.892	0.383
Variable	U	Anode	-0.003	-1.299	0.933
		Cathode	0.033	-1.859	0.795
	Pu	Anode	0.002	-1.311	0.471
		Cathode	-0.009	-1.768	0.092

From the values in Table 5.3, it is confirmed that the cathode has a greater sensitivity to the salt composition. Comparing the slope values of the cathode to that of anode, the cathode has an order of magnitude greater dependence on the composition in both the uranium and plutonium case except under the variable EXCD setting. The correlations, in general, are weaker when utilizing a variable EXCD. Thus using a fixed EXCD in an ER model could over-predict an expected change in the potential leading to false negative when attempting to detect SNM diversion.

It is interesting to note that the R^2 values are greater in the case of uranium composition. This would indicate that not only is plutonium deposition more tightly correlated with the uranium composition in the salt, but the electrode potentials are as well.

In regards to signatures, both the cell current and the cathode potential could be indicative of the diversion of plutonium via deposition of the cathode. Plutonium could be deposited on the cathode if the limiting current of uranium and other less active metals is exceeded. This could be caused by a reduction of the uranium inventory in salt, an increase in the cell current or both. Thus an elevated cell current could signal diversion.

The other signature – potential – has been shown to be dependent on the uranium inventory in the salt which is a controlling factor of plutonium deposition. By transitive logic, potential should be dependent of plutonium deposition. This is confirmed for a fixed EXCD in Figure 5.8 which contains a semi-log plot of the averaged cathode potentials against the amount of plutonium deposited on the cathode. However, this relation is not found for a variable EXCD. This could be the result of the increase in plutonium's EXCD with increasing plutonium deposition. As the EXCD of plutonium increases less overpotential is need to obtain the same partial current value. This offsets the decrease in potential due to a greater plutonium partial current. However, in both cases the potential drops when plutonium deposition occurs. Thus, a depressed cathode potential and elevate cell current would be a good signature of plutonium diversion, but a decreasing potential does not necessarily meaning an increasing plutonium partial current at the cathode.

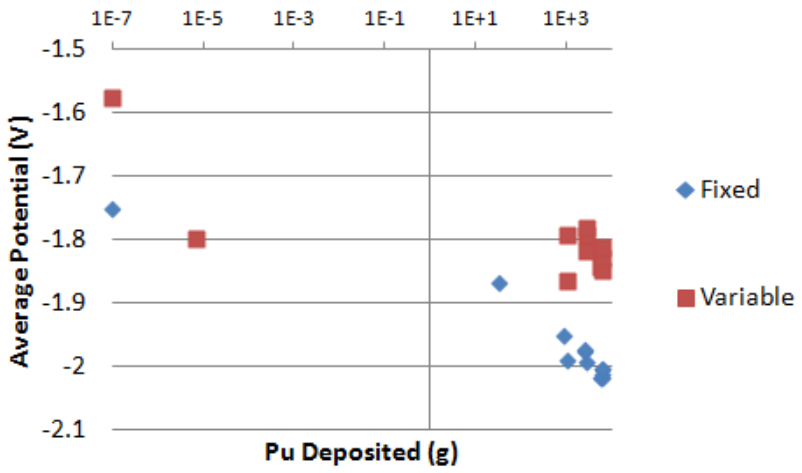

Figure 5.8 Plot of cathode potential against plutonium deposited on a semi-log plot

5.2.2 Comparison of constant and variable EXCD

Using a fixed or variable EXCD, can also affect the accuracy and identification of signatures. This is illustrated for one of the results of interest, plutonium deposition, in Table 5.4. The table displays the plutonium deposited for both EXCD settings and the difference between the two. In a separate table (see), the initial value of the variable EXCD for each case is provided. The initial values are shown for both uranium and plutonium because they are no longer fixed or equal.

Table 5.4 Comparison of plutonium deposition for variable and fixed EXCD of 0.5 A/m^2

Case number	1	2	3	4	5	6
Fixed EXCD	0	31.4	1014.98	893.35	2631.46	2604.41
Variable EXCD	0	6.77·10-6	1044.66	995.26	2711.21	2716.26
Difference (g)	0	31.4	-29.68	-101.9	-79.75	-111.85
Case number	**7**	**8**	**9**	**10**	**11**	**12**
Fixed EXCD	2597.85	5591.84	5915.57	5915.71	5916.83	5916.83
Variable EXCD	2726.61	5649.73	5969.75	5988.4	6005.08	---
Difference (g)	-128.76	-57.89	-54.18	-79.69	-88.25	---

Table 5.5 Variable EXCD values

Case number		1	2	3	4	5	6	7	8	9	10	11
Variable EXCD (A/m^2)	U	18.1	8.9	7.8	7.9	6.4	6.4	6.4	2.9	2.3	2.3	2.3
	Pu	4.5	4.5	7.6	18.7	19.6	28.3	34.5	23.6	23.6	28.3	33.6

As seen in Table 5.4, there is a difference in plutonium deposition between the two EXCD settings. However, the difference in the table could be overstated due to the large difference in EXCD values between the fixed and variable settings. Thus, noting the range of

the variable EXCD to be from 2.3 to 18.1 for uranium and 4.5 to 34.5 for plutonium, the cases were simulated with a fixed EXCD of 5 A/m^2 and the differences were recalculated based on the variable EXCD results in Table 5.4. The results for a fixed EXCD of 5 A/m^2 are displayed in Table 5.6.

Table 5.6 Comparison of plutonium deposition for a variable and fixed EXCD of 5 A/m^2

Case number	1	2	3	4	5	6
Fixed EXCD	0	23.61	1010.33	888.59	2627.70	2600.65
Difference (g)	0	23.61	-34.33	-106.67	-83.51	-115.61
Case number	**7**	**8**	**9**	**10**	**11**	**12**
Fixed EXCD	2594.08	5589.78	5913.70	5913.85	5914.97	5914.97
Difference (g)	-132.53	-59.95	-56.05	-74.55	-90.11	---

The difference is only decreased for case 2 which had both the variable EXCD of uranium and plutonium close in value to that of the fixed EXCD. However, as variable EXCD of plutonium increases the plutonium deposition values continue to diverge despite the decrease in the EXCD of uranium. This confirms that there is a difference due to the different treatments of the EXCD.

Another result affected by EXCD is the cathode potential. In Figure 5.2 and Figure 5.5, it is shown that the cathode potential profiles of fixed and variable EXCD have similar trends, but are at different potential values. The size of the shift in potential between fixed and variable EXCD is quantified in Table 5.7 by comparing averages of the potential profiles. The fixed EXCD value in the table below is 0.5 A/m^2. The potentials for a fixed

EXCD of 5 A/m^2 are consistently 0.08 V greater than the potentials for a fixed EXCD of 0.5 A/m^2.

Table 5.7 Comparison of the average cathode potential for a variable and fixed EXCD of 0.5 A/m^2

Case number	1	2	3	4	5	6
Fixed EXCD	-1.751	-1.867	-1.990	-1.951	-1.992	-1.976
Variable EXCD	-1.576	-1.798	-1.865	-1.794	-1.818	-1.793
Difference (V)	-0.176	-0.070	-0.125	-0.158	-0.174	-0.182
Case number	**7**	**8**	**9**	**10**	**11**	**12**
Fixed EXCD	-1.972	-2.016	-2.019	-2.013	-2.003	-2.003
Variable EXCD	-1.782	-1.842	-1.848	-1.828	-1.814	---
Difference (V)	-0.189	-0.174	-0.171	-0.184	-0.190	---

As demonstrated, the treatment of the EXCD can have an effect on the modeling and the prediction of potential especially for a diversion scenario in which the composition of the ER salt varies greatly. Because the fixed EXCD is generally lower than the variable EXCD in the PUR study, the potential predicted using a fixed EXCD is generally more negative and underestimates the amount of plutonium deposited when compared to the variable EXCD setting. This could lead to a false negative when monitoring the cathode potential for a signal of SNM diversion because the predicted potential needed for plutonium deposition would be more negative than the actual potential. In short, using a fixed EXCD limits the range within which accurate signatures can be predicted.

In summary, it has been established that current and potential are useful signatures of diversions. Uranium composition is a controlling parameter of these signatures and plutonium deposition. The EXCD is a critical variable in predicting the signatures values. A

variable EXCD is needed when modeling the ER over a large range of salt compositions which can occur in SNM diversion. The effect of the EXCD on potential diversion signatures is further examined in the next chapter.

6 Exchange Current Density Sensitivity Study

If the signature-based safeguards approach is to be employed, the model used for the ER needs to be able to accurately predict the values of the signatures for a range of ER conditions. In the previous section, cell current and cathode potentials have been identified as useful signatures for identification of plutonium diversion by deposition on a solid cathode. The EXCD is a highly uncertain value that affects both the cell current and cathode potential value predicted by ERAD and the other models. The effect of EXCD on these signatures is explored in this study.

Only Case 2 was examined (PUR of 0.091). Case 2 was selected because it captures the transition from uranium deposition to co-deposition. The EXCD of three species (uranium, plutonium and zirconium) varied between four values: 0.5, 5, 50 and 500 A/m^2. The three species selected were uranium, plutonium and zirconium because they contribute the most to the cell current and cathode potential. The minimum EXCD of 0.5 A/m^2 was chosen because it was the lowest value found in literature for uranium [8]. The maximum EXCD of 500 A/m^2 was chosen because it was on same magnitude as the EXCD determined for uranium in [27] and calculated from [28] (see Appendix B). Every combination of the species' EXCD was run resulting in 64 runs.

ERAD was set to the fixed EXCD setting for the study to allow control of the test variable. The results are still a good representation of reality because the concentration of a species varies little during a simulation. Specifically, in case 2, the changes in uranium and plutonium concentrations are 5.0% and 5.6% of the initial concentration values resulting in a similarly scaled change in the EXCD.

6.1 Calculation Results

The measure used to gauge the correlation between the EXCD of each species and plutonium deposition was the total plutonium deposited. The measure for the correlation of species' EXCD and cathode potential is more difficult due to the dynamic nature of the cathode potential. A representative cathode potential profile in Figure 6.1 illustrates the dynamics. The magnitude of the precipitous drop in the profile and the time of the drop are two things that are lost in a simple average of cathode. For this purpose, two statistics are used: the average and the range of cathode potential. The average potential gives a rough picture of the shift in potential due to changes in species EXCD. However, since uranium is predominately depositing, the effect of uranium's EXCD (U-EXCD) could mask the effect of others' EXCD. The range of the potential captures the drop of the cathode potential to allow plutonium deposition. Thus, the average highlights the effect of uranium's EXCD and the range highlights the effect of plutonium's EXCD (Pu-EXCD). The effect of Zirconium's EXCD (Zr-EXCD) is difficult to find due to its very small fraction of the cell current.

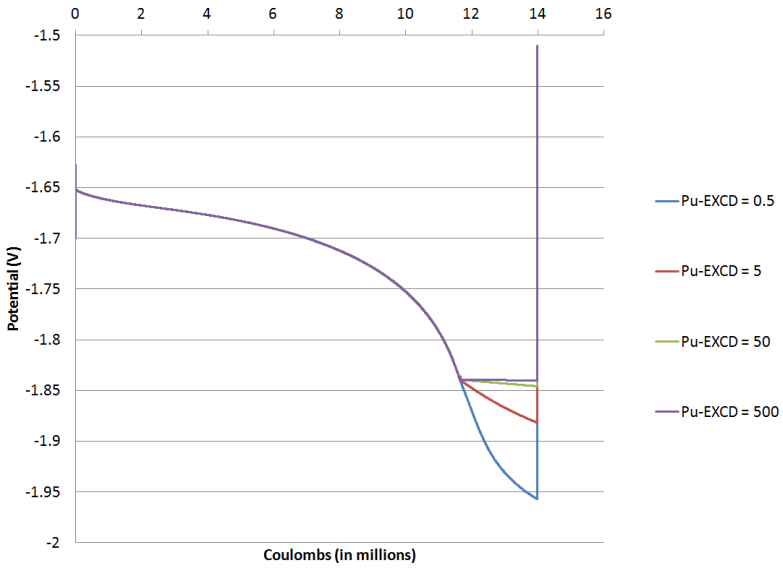

Figure 6.1 Typical cathode profile from EXCD sensitivity study

The effects of each species' EXCD on the three measures (total plutonium deposited, average potential, and range of the potential) were measured by obtaining the correlation coefficient. The correlation coefficients were determined using the Data Analysis Add-In in Microsoft Excel and are displayed in Table 6.1. These correlation coefficients only measure the linear dependence of two variables. However, they do give an indication of which parameters influence the given measure.

Table 6.1 Correlation coefficients for each species' EXCD

Correlation Coefficients			
Measure	U-EXCD	Zr-EXCD	Pu-EXCD
Pu Deposited (g)	-0.4221	0.08319	0.16173
Avg. Potential (V)	0.59576	0.07311	-0.10929
Potential Range (V)	0.75166	0.02332	-0.28087

The results in Table 6.1 show that uranium's EXCD has the greatest control over all three of the parameters. However, the correlation coefficient only determines the linear dependence of each measure on the species' EXCDs, further analysis is need to ensure that a dependence that exists is not overlooked and to determine the exact nature of the dependence.

Provided on the next two pages is a sampling of the results from the EXCD study to illustrate the effects of changing the EXCD. For a complete compilation of the results, see Appendix C. In Figure 6.2 and Figure 6.3, the plutonium deposited on the cathode and the cathode potential profiles are shown for select runs from the EXCD study. Four graphs are shown in each figure. In each graph there are four series which correspond to the plutonium EXCD values of 0.5, 5, 50 and 500 A/m^2. The left and right columns in the figures represent uranium EXCD of 0.5 A/m^2 and 50 A/m^2 respectively. The upper and lower rows in each figure represent zirconium EXCD of 0.5 A/m^2 and 50 A/m^2 respectively.

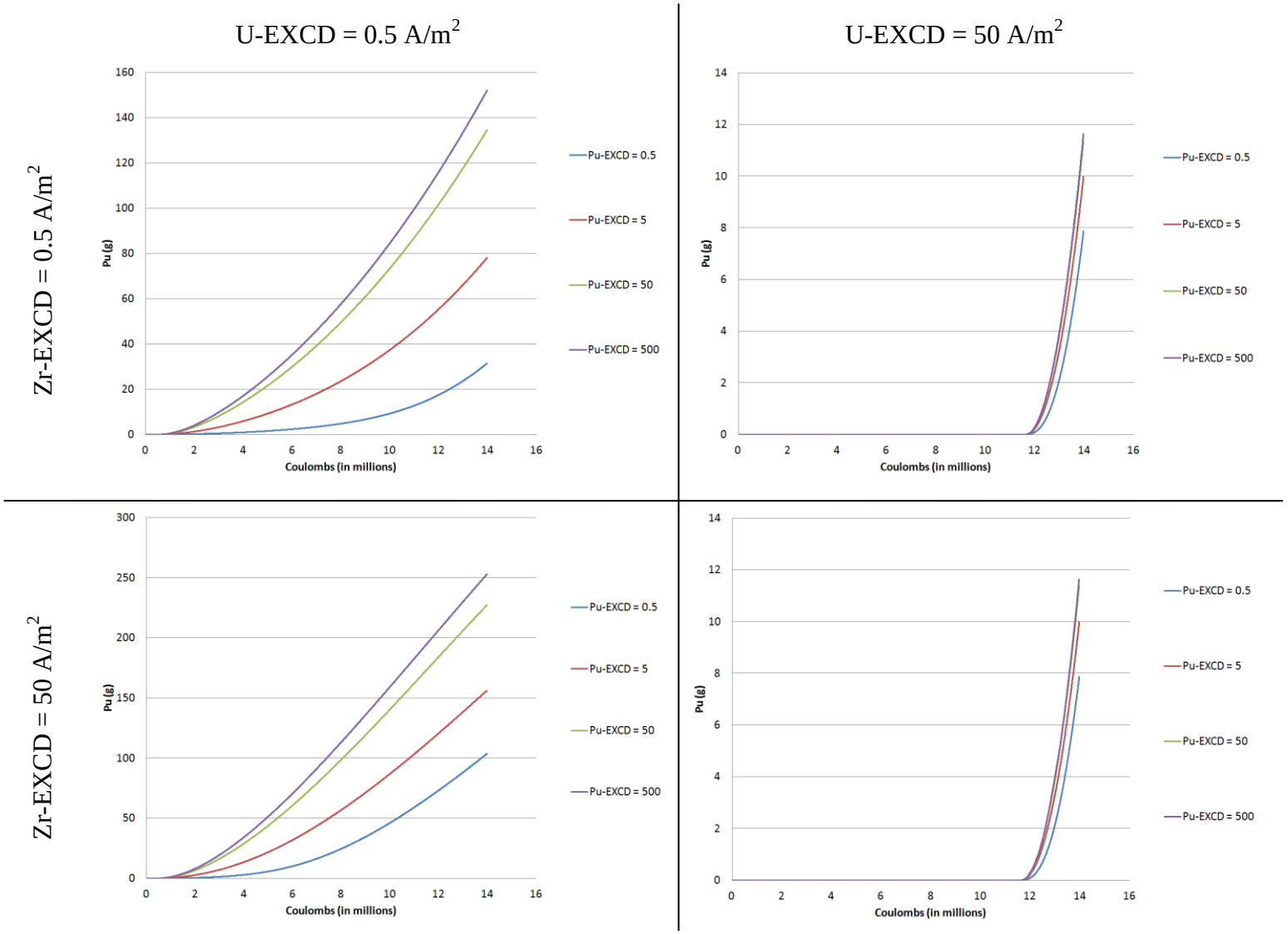

Figure 6.2 Plutonium deposition for select values of EXCD

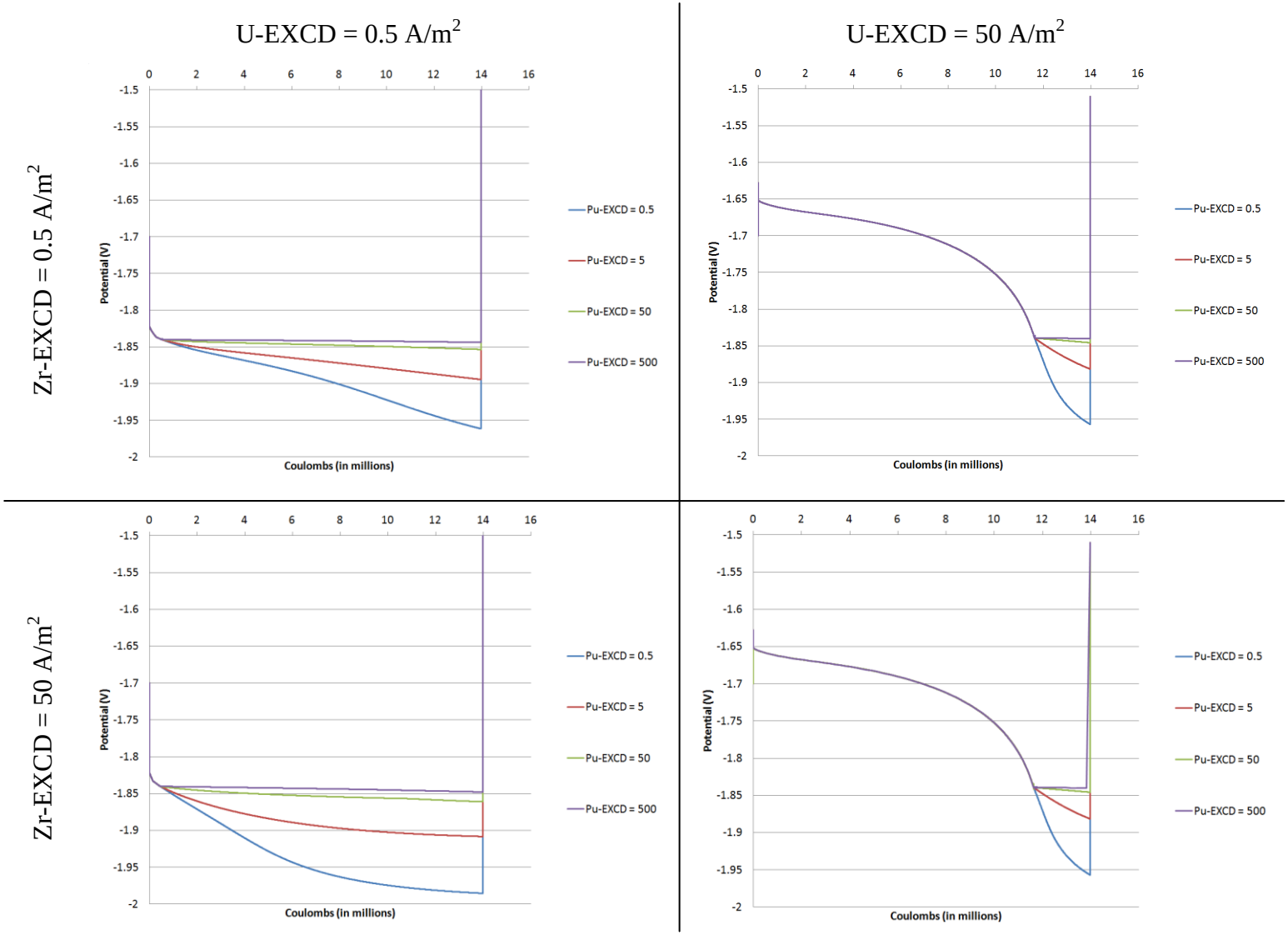

Figure 6.3 Cathode potential profiles for select values of EXCD

The first thing to note is that as the EXCD of plutonium increase the amount of plutonium deposited and cathode potential increases. Secondly, as the EXCD of uranium increases, plutonium deposition begins later in the simulation. When the uranium EXCD is 0.5 A/m^2, plutonium deposition begins shortly after starting the simulation. However, when the EXCD of uranium is elevated to 50 A/m^2, plutonium deposition doesn't begin until near the end of the simulation. Lastly, as the zirconium EXCD increases the amount of plutonium deposited increases and the cathode potential decreases. This is more evident when EXCD of uranium is lower.

Figure 6.2 and Figure 6.3 provide a good initial look at the effects of each species EXCD. However, a more detailed investigation requires the individual inspection of each species. The next few subsections look at the effects of each species' EXCD on the amount of plutonium deposited and cathode potential

6.1.1 Uranium's EXCD

6.1.1.1 Effect on Plutonium Deposition

In Figure 6.4, the plutonium deposited for all of the 64 runs is plotted versus uranium's EXCD on a log scale. This shows a strong decreasing trend with increasing EXCD of uranium. As seen in Figure 6.4, the amount of plutonium deposited varied by hundreds of grams.

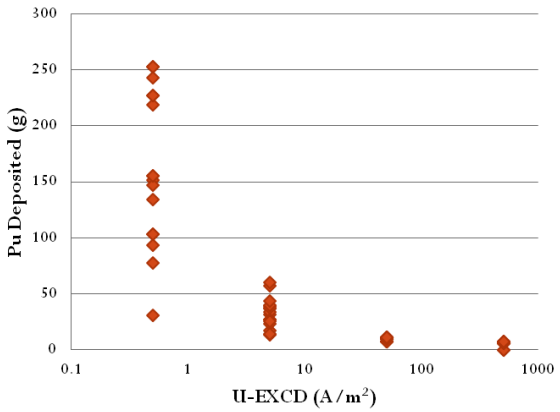

Figure 6.4 Plutonium deposited versus the EXCD of U with EXCD of Pu and Zr varying

The exact nature of this dependence can be determined by holding the EXCD of plutonium and zirconium constant. In Figure 6.5, the series with the EXCD of plutonium and zirconium fixed at 500 A/m^2 is fit to power law. The effect of uranium's EXCD on plutonium deposition weakens as the EXCDs of zirconium and plutonium decrease. This can be seen in Figure 6.5 by flattening of the curve as EXCD of zirconium and plutonium decrease.

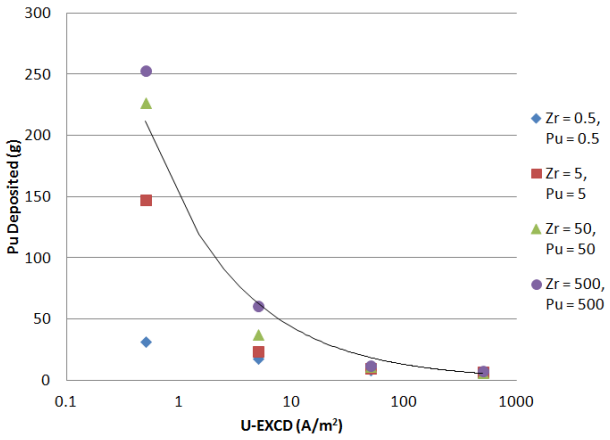

Figure 6.5 Plutonium deposited versus the EXCD of U with the EXCD of Pu and Zr fixed

The decrease in plutonium deposition with an increase in uranium's EXCD is in large part due to the reduced amount time that plutonium is depositing during the simulation. The trend of increasing the time at which plutonium deposition begins in the simulation is shown in Figure 6.6. This delay in initial plutonium deposition limits the time and amount of plutonium deposition during the simulation.

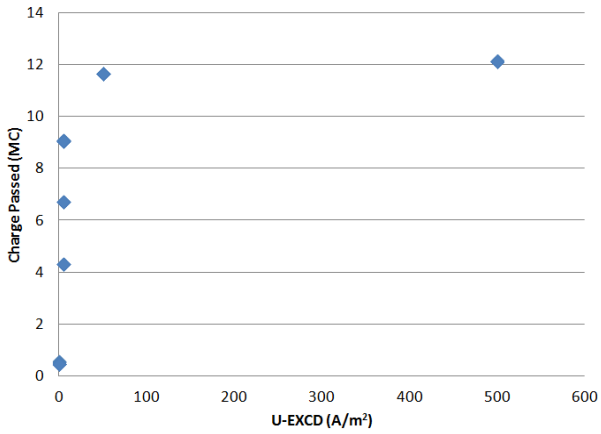

Figure 6.6 Amount of charge passed before plutonium deposition begin in a run

6.1.1.2 Effect on Cathode Potential

In Table 6.1, it is shown that for uranium an increasing EXCD results in an increased average cathode potential and range. The exact nature of this correlation is logarithmic as shown in Figure 6.7 and Figure 6.8. As seen in Appendix C, the EXCD of uranium increases the cathode potential profile when plutonium is not depositing. It also reduces the amount of time in the run that plutonium is depositing. These effects result in an increased average

cathode potential and an increased maximum cathode potential which increase the range if the EXCD of plutonium is held constant. The outliers in the individual series in the following graphs are due to abnormality in the runs (see Appendix D).

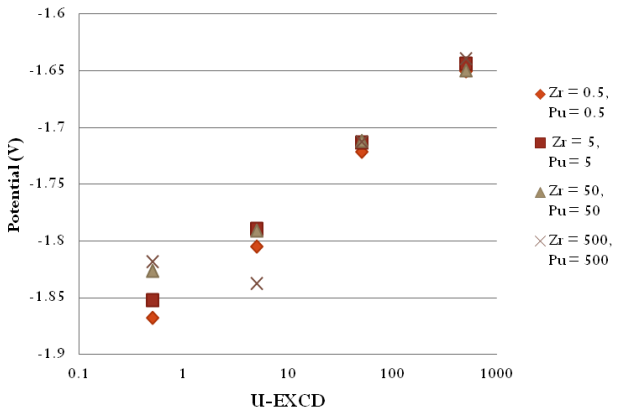

Figure 6.7 Average cathode potential versus EXCD of U with the EXCD of Pu and Zr fixed on a semi-log plot

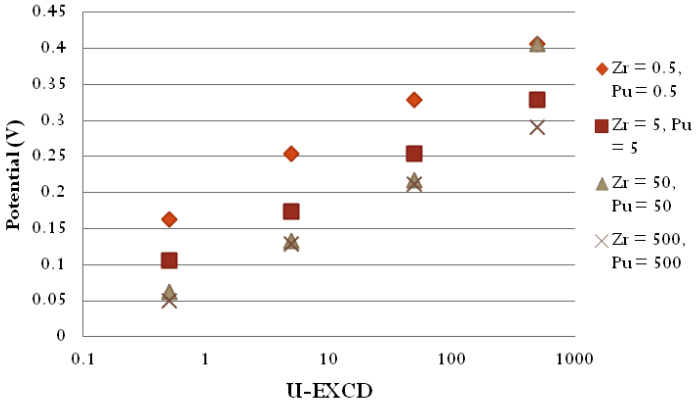

Figure 6.8 Range of the cathode potential versus the EXCD of U with EXCD of Pu and Zr fixed on a semi-log plot

6.1.2 Plutonium's EXCD

6.1.2.1 Effect on Plutonium Deposition

In Table 6.1, it is shown that an increase in the EXCD of plutonium results in an increase of plutonium deposited. In Figure 6.9, the relationship between plutonium deposited and EXCD is logarithmic and most pronounced when the other species' EXCD are low.

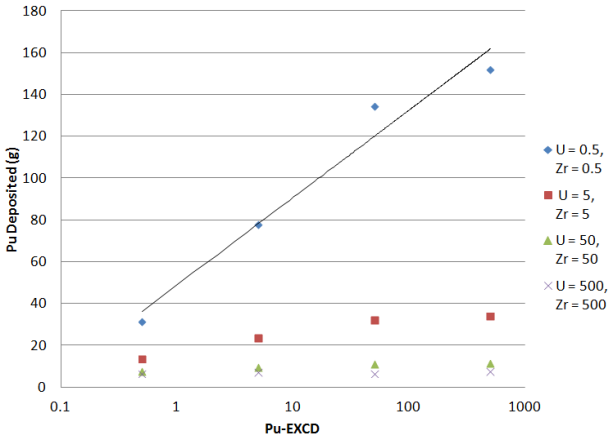

Figure 6.9 Plutonium deposited versus the EXCD of Pu with the EXCD of U and Zr fixed on a semi-log plot

6.1.2.2 Effect on Cathode Potential

By inspecting the plots in Appendix C, it is apparent that an increase in the EXCD of plutonium increases the cathode potential, but only while plutonium is depositing. Thus the effect of plutonium's EXCD on the average cathode potential is diminished as uranium's EXCD increases, as shown in Figure 6.10. When the EXCD of other species is fixed at 0.5

A/m^2, plutonium has the strongest effect on the average cathode potential because plutonium is depositing nearly the entire time in those simulations. The two outliers in the series with fixed EXCDs of 5 and 50 A/m^2 are due to irregular data reduction.

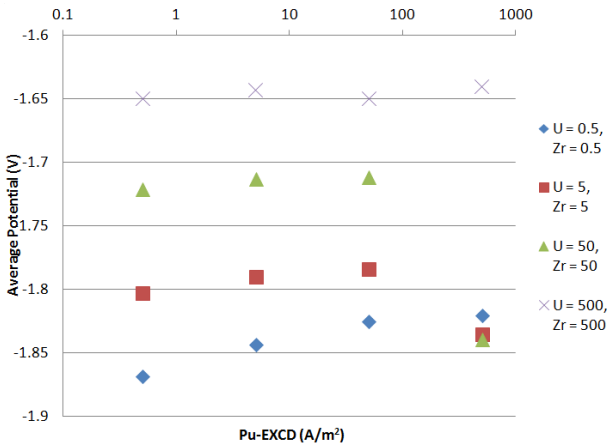

Figure 6.10 Average cathode potential versus the EXCD of Pu with the EXCD of U and Zr fixed on a semi-log plot

The EXCD of plutonium also has an effect on the range of cathode potential Figure 6.11 shows that the correlation between cathode potential and the EXCD of plutonium is logarithmic. However, plutonium's EXCD has a decreasing trend because as plutonium's EXCD increases, the minimum cathode potential increases (see Appendix C). Again, the outlier in the series with a U-EXCD and Zr-EXCD of 500 A/m^2 is due to an abnormal run.

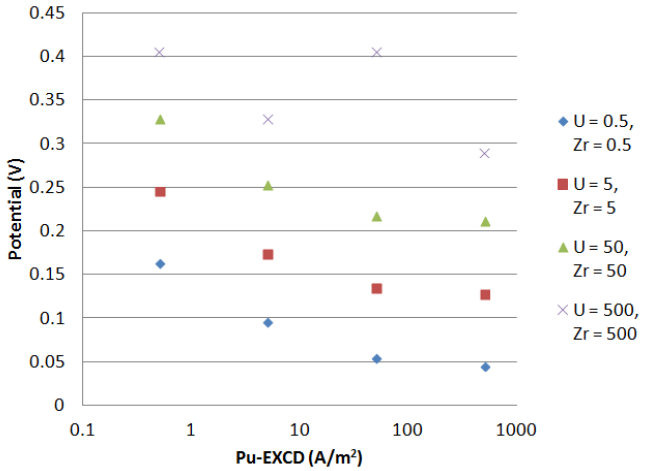

Figure 6.11 Range of the cathode potential versus the EXCD of Pu with EXCD of U and Zr fixed on a semi-log plot

6.1.3 Zirconium's EXCD

While no significant correlation exist for Zirconium's EXCD according to Table 6.1, it does affect the amount of plutonium deposited. This effect is shown in Figure 6.12. The EXCD values for uranium and plutonium are fixed at 0.5 A/m^2 while zirconium increases from 0.5 to 500 A/m^2. This occurs at other values of uranium's and plutonium's EXCD, but is less pronounced (See Appendix C).

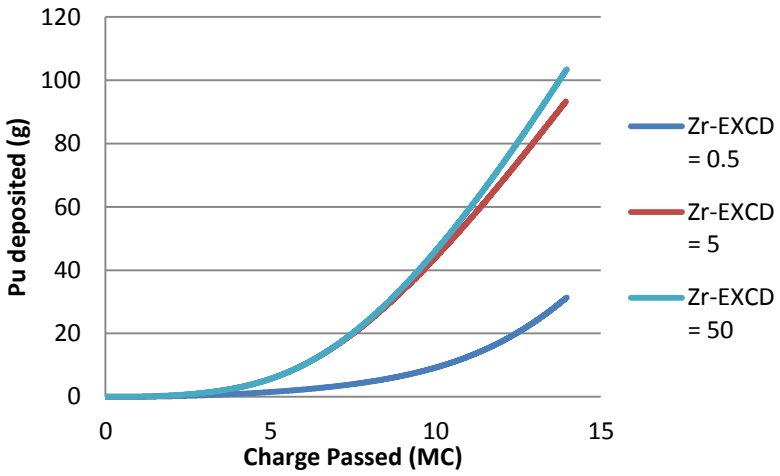

Figure 6.12 Plot of plutonium deposition on cathode at U-EXCD and Pu-EXCD equal to 0.5 A/m^2

6.2 Discussion

It was noted that increasing the EXCD of uranium resulted in the delay of plutonium deposition in the simulation. This is due to a decrease in the depletion rate of uranium in the salt inventory as the EXCD of uranium increases (see Figure 6.13). The increased EXCD of uranium allows for it to account for more of partial current at the anode while deposition of uranium at the cathode remains fixed, if it is the only species depositing. With the decrease in net removal rate of uranium from the salt, it requires more time for the limiting current to drop below the requested cell current.

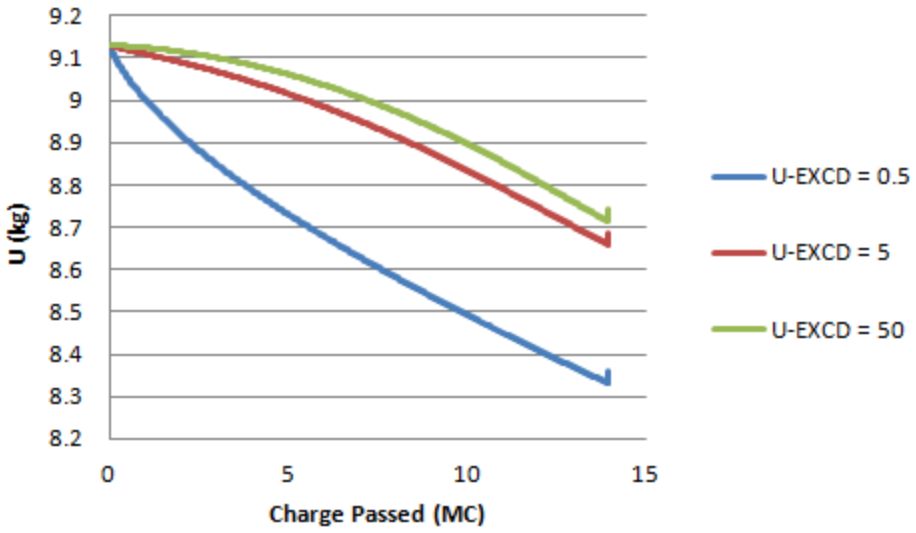

Figure 6.13 Salt inventory of uranium for a fixed EXCD of 0.5 A/m^2 for Pu and Zr

Another finding from the study is that an increase in the EXCD for any species results in an increase in the cathode potential (i.e. less negative). The current of each species is related to the cathode potential by overpotential in the Butler-Volmer equation, (2.18). An increase in EXCD decreases the magnitude of the overpotential (i.e. less negative) which in turn makes the cathode potential less negative.

The finding that zirconium's EXCD can actually have positive effect on plutonium deposition is due to same reason for a decrease in plutonium deposition with an increase in the EXCD of uranium. That is an increase in the EXCD of zirconium results in an increase of its partial current at the anode. This is confirmed in Figure 6.14 which shows an increased removal of zirconium from the anode. This increase in the partial current of zirconium crowds out the other species resulting in less uranium being oxidized. This increases the

depletion rate of uranium in the salt which causes plutonium deposition to occur earlier in the run.

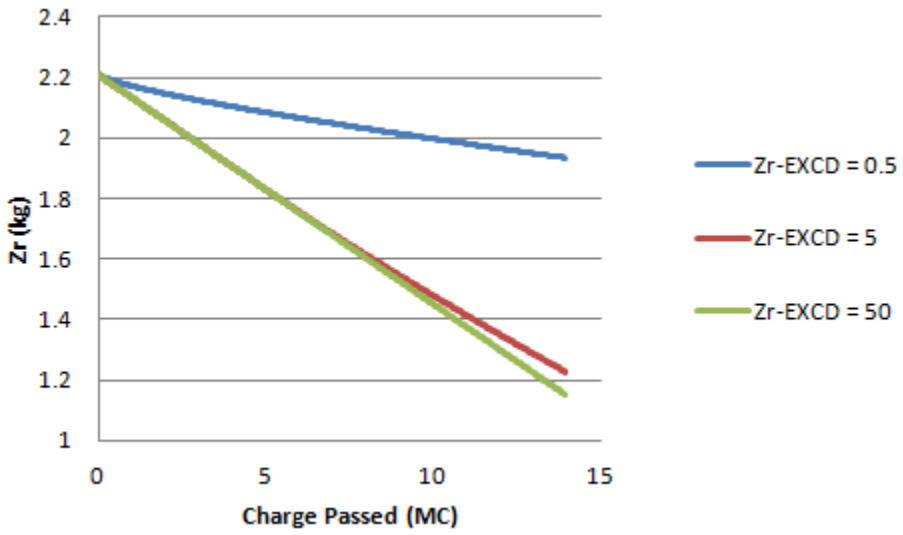

Figure 6.14 Anode inventory of zirconium for a fixed EXCD of 0.5 A/m^2 for U and Pu

The amount of plutonium deposited only varies by a couple hundred grams over an approximately 39 hour time period for a wide range of EXCD values. This is well within significant quantity limit of 8 kg for plutonium by the IAEA. Based on the maximum difference in plutonium deposition in this study, it would require 52 days before the error in the prediction exceed a SQ of plutonium. This could be tolerable depending on the turn-around of DA results on the feed and salt inventories.

It is important to note that this study was done on an engineer-scale ER at a cell current of 100 A. Industrial–scale facilities would have a greater throughput which could increase the inventory discrepancy caused by an erroneous EXCD more rapidly. One possible means of

increasing the throughput is to increase the operating cell current. By increasing the cell current by 5 A, the maximum discrepancy increased such that the time required to divert 1SQ of plutonium decreased by 6 days.

6.2.1 Relative EXCD of Uranium and Plutonium

The relative EXCD of uranium and plutonium when plutonium deposition begins is of particular interest for the detection of SNM diversion. The relationship of two species' (U and Pu) EXCDs can be found by taking the ratio of the two EXCDs. Using (2.13) and (2.16) the ratio is determined.

$$\frac{i_{o,U}}{i_{o,Pu}} = \frac{n_U \cdot F \cdot k_U^o \cdot C_{U^{3+}}^{(1-\alpha)} \cdot {C_{U^{3+}}^o}^{\alpha}}{n_{Pu} \cdot F \cdot k_{Pu}^o \cdot C_{Pu^{3+}}^{(1-\alpha)} \cdot {C_{Pu^{3+}}^o}^{\alpha}} = \frac{k_U^o \cdot C_{U^{3+}}^{(1-\alpha)}}{k_{Pu}^o \cdot C_{Pu^{3+}}^{(1-\alpha)}}$$

If the concentrations at which the standard rate constants are determined are the same for each species, then the ratio only depends on the standard rate constant and oxidized species concentrations. Cumberland and Yim estimated the standard exchange current densities of uranium and plutonium to be 40 – 100 and 30 – 100 A-m$^{-0.5}$-mol$^{-0.5}$ respectively [29]. Thus, because the number electrons transferred are equivalent, it is most plausible that their standard rate constants, k^o, are approximately equal. Under such an assumption, the ratio of EXCDs would be equal to the ratio of the bulk molten salt concentrations.

In terms of proliferation, the operating condition of concern is a high plutonium concentration and low uranium concentration in the salt. This would correspond to a high plutonium EXCD and a low uranium EXCD. Unfortunately, in this case, the transition from uranium deposition to co-deposition of uranium and plutonium is the least pronounced in the

cathode potential. This is illustrated in Figure 6.15 which compares the cathode potential profiles from a case with a low U-EXCD and high Pu-EXCD to a case with high U-EXCD and low Pu-EXCD. The low EXCD setting is 0.5 A/m^2 and the high EXCD setting is 50 A/m^2. In both cases the EXCD of zirconium is 0.5 A/m^2. The arrows in the figure indicate with which x-axis the series coincide. The contrast of the two cases in Figure 6.15 demonstrates the relative potential drop from normal operation to co-deposition. As shown, the potential drop for the most likely relative EXCD scenario of co-deposition on a solid cathode is much smaller than the opposite EXCD scenario.

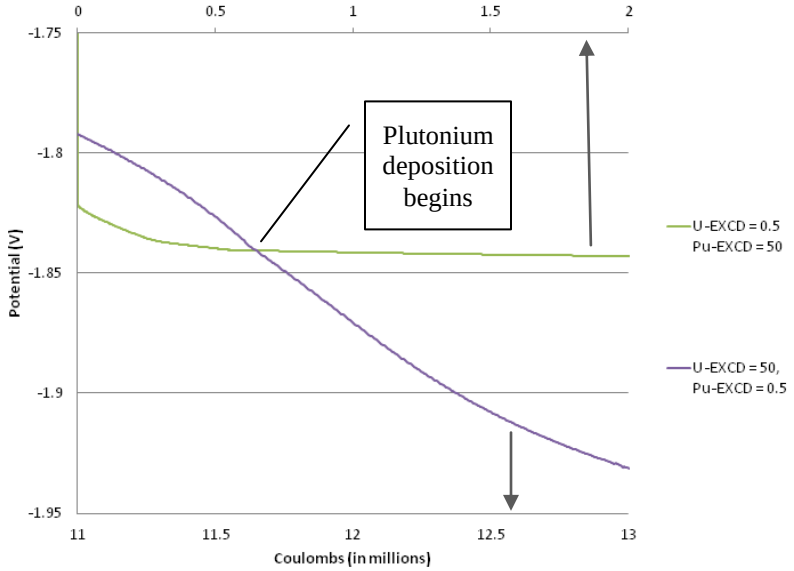

Figure 6.15 Cathode potential profile at the transition to co-deposition of U and Pu

The less pronounced potential drop would require greater sensitivity in detecting the potential at which plutonium deposition commences. A better accuracy of each species

EXCD would aid in increasing the accuracy of predicting the time and potential at which plutonium deposition occurs.

In summary, the accuracy of the EXCD does not significantly impact the amount of plutonium deposited on an engineering scale. An EXCD estimate accurate to an order of magnitude should be sufficient to keep inventory discrepancies manageable over prolong periods. However, the sensitivity of the product composition on the EXCD increases as cell current increases necessitating greater accuracy of EXCD on the industrial scale. More importantly, the EXCD impacts the cathode potential and could result in the untimely detection of the co-deposition of plutonium on the cathode with uranium.

7 Proposed Method for Signature-Based Safeguards

The combination of cell current and cathode potential have been identified as signatures to detect the diversion of plutonium via co-deposition on a solid cathode. Previous models [8, 23, 24] require knowledge of the initial compositions of the electrolyte in the ER and SNF in the anode to determine the deposition rate of each species at the cathode. The objective of this method is to remove the necessity of knowing the initial compositions. Although, as the previous chapter illustrated, some fundamental parameters need to be better characterized; this chapter demonstrates the methodology whereby the cell current and cathode potential are combined to predict the species being deposited on the cathode without previous knowledge of the ER compositions.

7.1 General Approach

This approach utilizes two features of electrorefining. First, it requires a large amount of charge to reduce a mole of a species. In the specific case of uranium and plutonium, it requires 289,455 coulombs. Second, the large volume of material in the bulk molten salt requires significant change in composition to affect the concentrations. Consequently, if the current is low, the bulk concentrations of species could be considered constant over a small amount of charge passed. This obviously has limitations, most significantly high currents and small bulk concentrations of species. The first limitation can treated by reducing the current to a low value to apply the analysis proposed in this method. The second limitation is not a concern with plutonium because the bulk concentration of plutonium needs to be high for deposition to occur.

As mentioned, this new approach requires the electrorefiner current to be reduced to zero or near zero. This allows for the concentrations to be assumed constant. Figure 7.1 shows an example of the required current profile to determine the deposition rates for two species reacting at the cathode. First, the system is at its normal operating current (I_{op}). Then the current is dropped to zero. Next, the current is stepped up to a value (I_{step}) near zero. Subsequently, the system is returned to its operating current. This current profile would produce the corresponding potential profile in Figure 7.1. Using the current profile on the next page, or one similar, the deposition rates of the species in an electrorefiner can be determined.

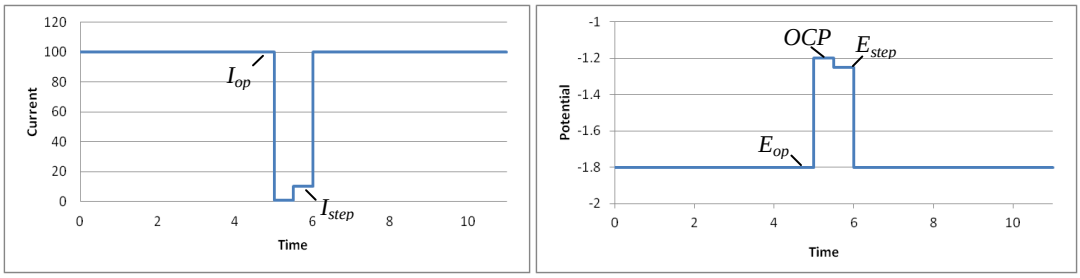

Figure 7.1 Example current and potential profiles for the application of deposition model for two species

This method uses a modified version of the B-V equation to determine the deposition rates of each species. In (2.19), the B-V equation is dependent on species' concentration and overpotential. However, using (2.2), (2.3) and (2.4), the overpotential is made a function of concentration, as shown below.

$$\eta_{j,k} = E_k - E_j^o + \frac{\nu \cdot R \cdot T}{n_j \cdot F} ln\left(\frac{\gamma_{j^{n+}} \cdot C_{j^{n+}}}{C^o}\right) \tag{7.1}$$

The subscript k indicates the current step. Substituting (7.1) into (2.19) makes the species current a function of the bulk and surface concentration. The surface concentration can be eliminated by using (2.22) resulting in (7.2).

$$I_{j,k} = \frac{A \cdot i_{o,j}^o \cdot \left[e^{\frac{\alpha_j \cdot n_j \cdot F}{R \cdot T}\left(E_j^o - E_k\right)} - \frac{\gamma_{j^{n+}} \cdot C_{j^{n+}}}{C^o} \cdot e^{-\frac{(1-\alpha_j) \cdot n_j \cdot F}{R \cdot T}\left(E_j^o - E_k\right)}\right]}{\frac{\gamma_{j^{n+}} \cdot i_{o,j}^o \cdot e^{-\frac{(1-\alpha_j) \cdot n_j \cdot F}{R \cdot T}\left(E_j^o - E_k\right)}}{C^o \cdot n_j \cdot F \cdot h_j} + 1} \tag{7.2}$$

Thus at each low current setting or step, a species' current is dependent on its concentration and the cathode potential. The cathode potential is measured leaving only the bulk concentrations as unknowns. The total, or cell, current serves as a constraint in this method.

By applying (2.20) to this method, a constraint is developed for each current step as shown below.

$$I_{T,k} = \sum_{j} I_{j,k}\left(C_{j^{n+}}, E_k\right) \tag{7.3}$$

The bulk concentration of the species at each low current step is considered constant and the cathode potential is measured at each current step. Consequently, each additional low current step adds a constraint, but no new unknowns. Thus, in order for the solution to converge, the number of current steps needs to be equivalent to the number of species actively depositing on the cathode.

The process used to solve for the rates is outlined in flowchart on the next page (see Figure 7.2). Throughout the description of this process, there are numbers in parenthesis. These numbers coincided with the numbers in Figure 7.2.

The process initiates by assuming that only uranium is deposited. This is referred to as "normal" operation. (1-2) If that is the case, then it is a simple calculation to determine the bulk concentration of uranium at the cathode's open-circuit potential (OCP) which (3) then can be used to determine the cell current at the operating potential (E_{op}). If this value matches the measured cell current at E_{op} then the measured current is the deposition rate of uranium. Otherwise, an additional measurement is required to determine the deposition rates. (4) The current is stepped up from zero current to a low current to which corresponds a potential, E_{step} . (5) The concentration of the side reactant is determined at the OCP utilizing the concentration of uranium and the fact that the sum of the two currents must be zero at the OCP. Now, there are guesses for the concentrations of the two species. (6) The cell current

at E_{step} is calculated based of the concentration guess values. If the calculated current does not match the measured current at E_{step}, then (7) the concentration of uranium is incremented up or down depending on whether the side reactant is less or more noble. Subsequently, the process is looped back to step 5. (8) If the concentration guesses are accurate then the cell current is determined at E_{op}. If this calculated cell current does not converge to the measured current then there are few reasons for the discrepancy. (9) The error could be due to an additional side reaction in which case the process is looped back to step 4 and an additional low current step is made. On the other hand, the species selected for the side reaction could have been incorrect in which case the side reactant is changed and no additional current step is needed.

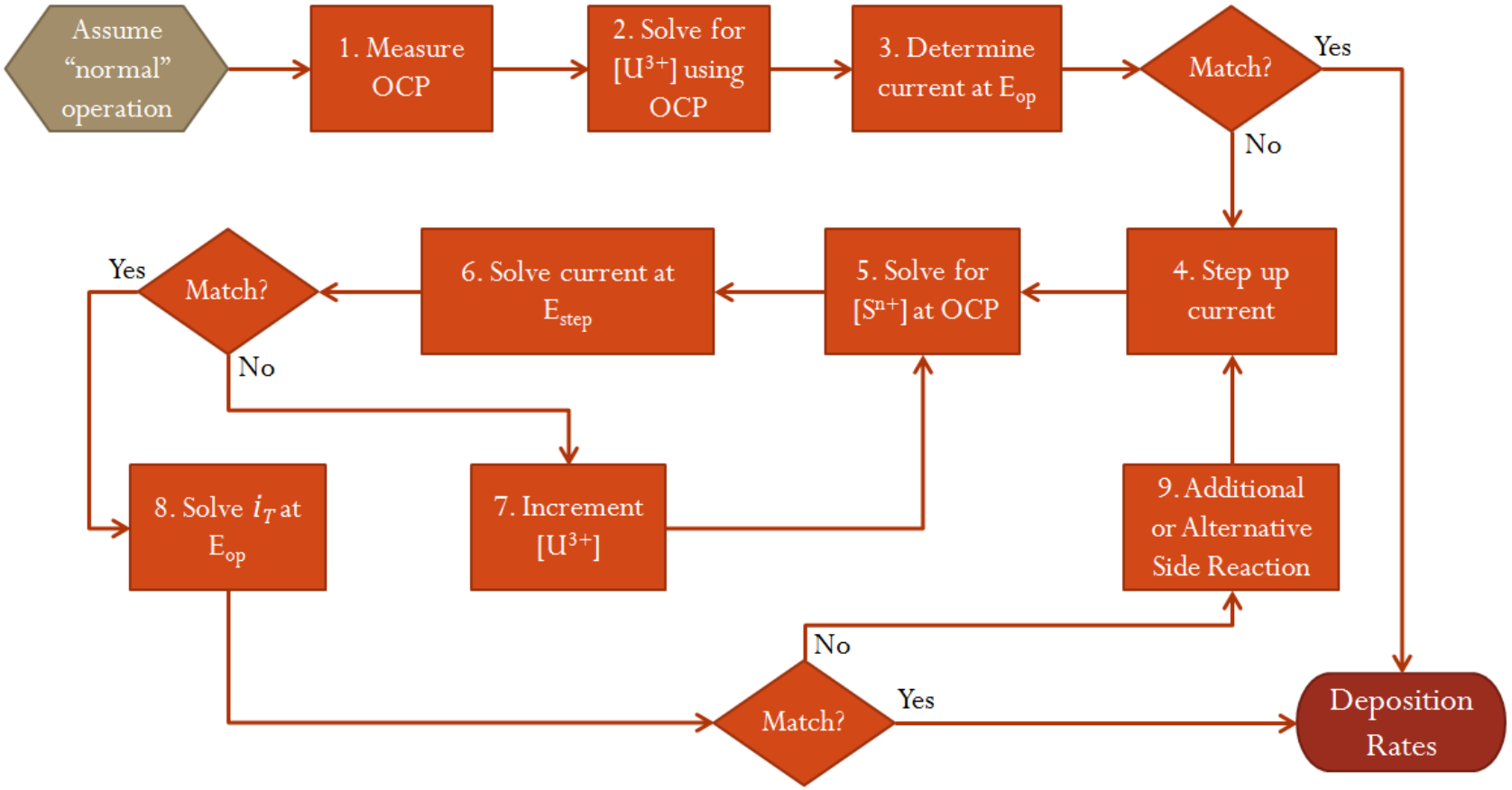

Figure 7.2 Flowchart of solving method for the determination of deposition rates from cell current and cathode potential

7.2 Model Development

A model was developed to predict the species deposition rates at the cathode using the general approach outlined above. The complete code and user interface for the model is provided in Appendix E. The code was written using Visual Basics for Applications (VBA) in Microsoft Excel 2007. The model uses (7.2) and (7.3) to solve for the bulk concentration. Based on the bulk concentrations, the deposition rates of uranium and plutonium are determined.

As shown in (7.2), the premise of this model is based on reducing each species current to depend solely on the bulk concentration and the cathode potential. However, the activity coefficients of the major constituents of SNF were determined with respect to mole fraction [8, p. 27]. In order to convert concentration to mole fraction, X, it requires knowledge of each major species concentration in the salt. This counteracts the object of determining the deposition rates without complete knowledge of the ER compositions. Thus, for the purposes of this initial modeling attempt, an alternative activity coefficient, γ^*, was determined by equating the activity with respect to the mole fraction and the activity with respect to the concentration, as shown below.

$$\gamma_{j^{n+}} \cdot X_{j^{n+}} = \frac{\gamma^*_{j^{n+}} \cdot C_{j^{n+}}}{C^o} \tag{7.4}$$

The alternative activity coefficient was determined at each case in the PUR study by using the salt compositions determined in ERAD. An average of the resulting activity coefficients

was used for each species in the model. Ideally, when applying this model to an actual ER, the activity coefficients with respect to concentration would be experimental determined.

Additionally, the mass-transfer coefficient needed to be characterized because ERAD solved the mass-transport equation, (2.21), as opposed to (2.22). The mass-transfer coefficient is commonly taking as the diffusion coefficient divided by the diffusion layer thickness, δ.

$$h_j = \frac{D_j}{\delta} \tag{7.5}$$

Alternatively, a mass-transfer correlation can be developed for the ER based on its geometry which allows for the mass-transfer of each species to be determined based on the rotational velocity (ω) of the electrode. For example, rotating cylindrical electrodes have the following mass-transfer correlation [30, pp. 164-167, 8, pp. 33-37].

$$Sh = \frac{h_j \cdot d}{D_j} = 0.0791 \cdot Re^{0.7} Sc^{0.356} = 0.0791 \cdot \left(\frac{d^2 \cdot \omega}{\nu}\right)^{0.7} \left(\frac{\nu}{D_j}\right)^{0.356} \tag{7.6}$$

where d is the diameter of the inner electrode and ν is the kinematic viscosity of the electrolyte. For simplicity, a mass-transfer coefficient was determined for the model by fitting the bulk and surface concentration data from ERAD across the salt compositions in the PUR study, essentially assuming that the coefficient is well characterized by one of the previously mentioned methods. The mass-transfer coefficient was fitted using the values at the operating (100 A) and low (5 A) currents. The values for the mass-transfer coefficient at the zero and five amp settings were the same. The fit of the mass-transfer coefficient for uranium and plutonium is shown in Figure 7.3.

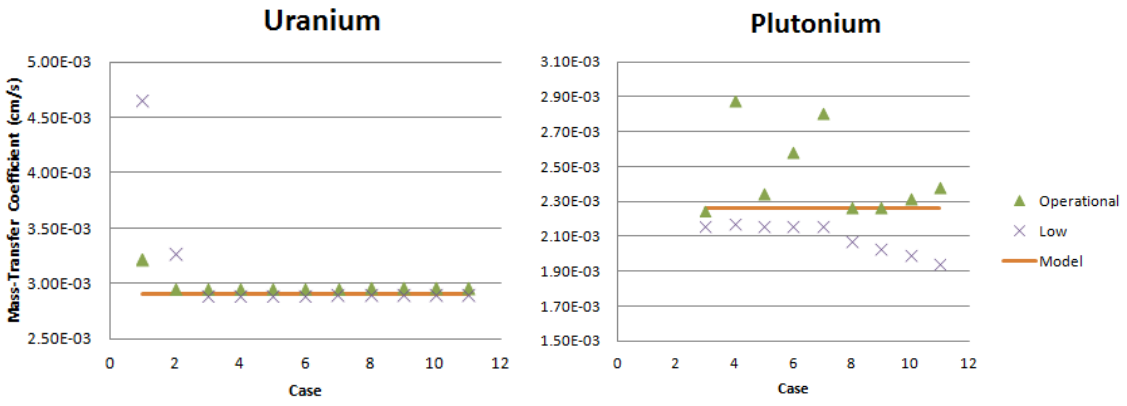

Figure 7.3 Fit of mass-transfer coefficient from ERAD data

Lastly, the treatment of the area term was simplistic. Each species was assumed to react uniformly over the entire surface area of the cathode. The surface area of the cathode was assumed to be constant.

7.2.1 Limitations

As is the case with most models, there are limitations to this model's applicability as currently developed. Further development could address these issues. The limitations currently known are: (1) number of species, (2) low current steps, and (3) solid cathode only.

The first three limitations are related. The number of species is limited because the steps need to be large enough to create an appreciable difference in the calculations, but the current has to be low enough to maintain the assumption of constant bulk concentrations. This limits the number of steps that can be made which is directly related to the number of species. Also, the model can only determine the concentration of the species actively reacting at the cathode. These limitations could be addressed by allowing the concentration to be

dynamic between each current step. This would require the calculation of the change in concentration between current steps, k, which could be done by the following equation.

$$C_{j,k} = C_{j,k-1} + \frac{i^a_{j,k-1} - i^c_{j,k-1}}{V \cdot n_j \cdot F} \cdot \Delta t_{k-1} \tag{7.7}$$

where V is the volume of the salt phase in the ER and Δt_{k-1} is the time elapsed at previous current step. This requires the partial current of each species to be determined at both the anode and cathode. Thus an analysis of the anode potentials would be needed.

The last limitation of a solid cathode can be resolved by taking two current steps per species. A liquid cathode would require knowledge of the concentration of the reduced species in the cathode because the activity in the cathode phase can no longer be assumed to be unity. This introduces an additional unknown requiring an additional data point.

7.3 Results

The results of the model were compared to the ERAD calculations to test the theoretical basis of the model. ERAD was run at each composition setting from the PUR study using a variable EXCD with a modified current profile. The current was set to 100 A for 2 hours, then dropped to 0 A for 3 minutes, and subsequently raised to 5 A for 3 minutes. The potential at each current setting was recorded and fed to the model to predict the deposition rates of uranium and plutonium at the cathode.

The concentration of both uranium and plutonium calculated by ERAD at the 2-hour point was compared to the concentrations predicted by the model. The absolute errors between the concentrations are plotted in Figure 7.4.

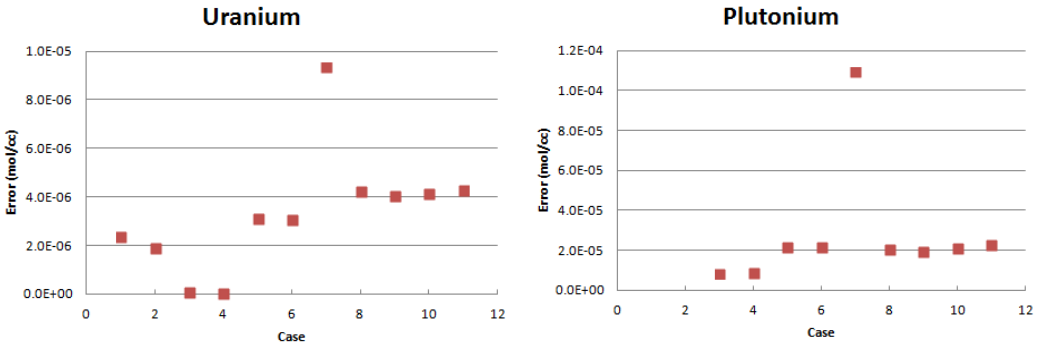

Figure 7.4 Absolute error between predicted and ERAD concentrations

The error minimizes at cases 3 and 4, and then gradually rises with exception of case 7 which is an outlier. Also, the error for the plutonium concentration is an order of magnitude larger than the error for uranium. The error relative to the calculated ERAD values ranges from 0.04% - 21.69%. Cases 1 and 2 are not included for plutonium because it is not actively depositing on the cathode which prevents the concentration from being determined.

Additionally, the absolute errors for the deposition rates at the 2-hour point were determined and are displayed in Figure 7.5. The errors are on the same magnitude for both uranium and plutonium, though the plutonium error is greater. Again, case 7 is an outlier. The relative errors of the deposition rates range from 0.18-21.0%. For completeness, the concentrations, deposition rates and errors from ERAD and predicted by the model are shown in Appendix F.

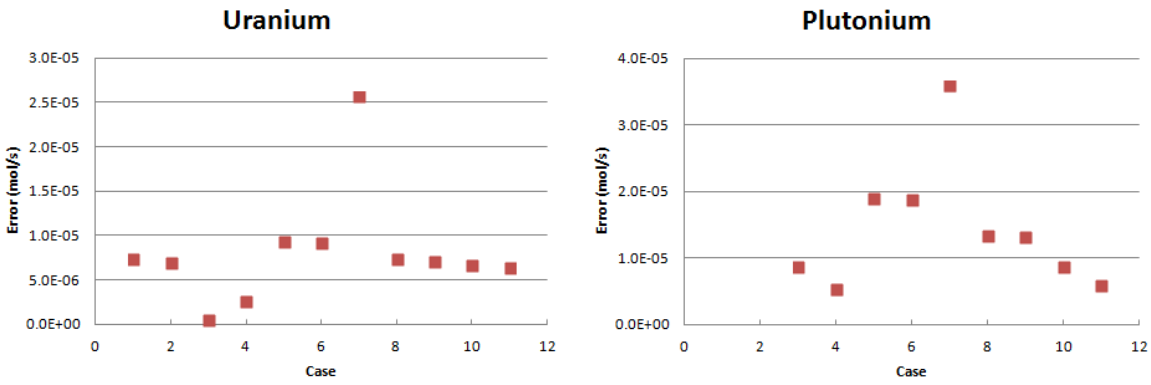

Figure 7.5 Absolute error between ERAD and predicted deposition rates

7.4 Discussion

Case 7 was a consistent outlier in terms of its absolute error. This exact cause of this error is not known. However, the mass-transfer coefficient at the operating current shows a large discrepancy from the model value which could cause the large error in the results. While a similar discrepancy is shown for case 4, plutonium deposition is only accounts for a small fraction of the operating current. In case 7, plutonium deposition accounts for roughly half of the operating current.

This initial attempt at combining the cell current and cathode potential to predict the deposition of the species at cathode proved to be effective. The deposition of plutonium was detected, even in case 3 when plutonium deposition is significantly less than uranium deposition. Although the treatment of many aspects of the ER was rudimentary, the predicted values followed the trends of and were comparable to the ERAD calculations. This demonstrates that the model is indeed theoretically consistent with ERAD, but parameters could be better calibrated.

8 Conclusion

Pyroprocessing is not completely immune to the diversion of SNM requiring the application of safeguards to the process. Several methods and techniques of monitoring and safeguarding pyroprocessing have been proposed among which is Signature-Based safeguards. Potential signatures identified for the specific diversion scenario of plutonium co-deposition on a cathode are a depressed cathode potential and an elevated cell current. Using the combination of the signatures, cell current and cathode potential, a method was devised in which the deposition rates of uranium and plutonium on the cathode could be determined. A model was developed to demonstrate this method. The model predicted deposition rates of uranium and plutonium based on the cell current and cathode potential values without any knowledge of compositions in the electrorefiner. The predicted deposition rates were comparable to the calculated rates in ERAD validating the theoretical basis of the method derived in this work. The ability to predict the deposition rates without accurate former knowledge of the electrorefiner's composition enables real-time monitoring of the flow of material in the electrorefiner, particularly the flow of material from the salt onto the cathode.

In development of the model, certain parameters needed to be estimated or assumed. The accuracy of the predicted deposition rates can be improved by better characterization of the EXCD, mass-transfer coefficient, reaction area of each species and the activity coefficient. The sensitivity of one of these parameters, ECXD, on deposition rates was investigated. Both the amount of plutonium deposited and cathode potential are affected by the EXCD. While affected by the EXCD, the amount of plutonium deposited on the cathode

does not show a significant difference with varying EXCD values at the engineering-scale. On the other hand, the EXCD introduces an error in the prediction of the cathode potential that could result in inaccurate and untimely detection of plutonium deposition on the cathode.

Additional work can be performed using the method and model devised in the work. First, experimental validation of the model needs to be performed to test its assumptions and applicability to the electrorefining of SNF. The model could potentially be applied to other diversion scenario, electrorefiner configurations or product optimization. For example, the cathode potentials and cell current could be monitored to enhance product purity by detecting the co-deposition of zirconium or other impurities. Additionally, model parameters and settings can be investigated to determine optimal values and configurations. Sensitivity studies on other modeling parameters could be done to help guide experimental work being done to characterize electrochemical properties. The model could be further developed to remove the low current requirement to allow larger or more current steps. Removing the low current requirement would also reduce the interference of the model on actual process operations. Moreover, the removal of the low current constraint would allow for an inspector or operator to use a few measurements of the cell current and cathode potential to determine the species actively depositing at the cathode.

REFERENCES

[1] R. Bean, "Project Report on Development of a Safeguards Approach for Pyroprocessing," Idaho National Laboratory, Idaho Falls, ID, 2010.

[2] L. W. Niedrach and A. C. Glamm, "Uranium Purification by Electrorefining," *Journal of the Electrochemical Society,* vol. 103, no. 9, pp. 521-528, 1956.

[3] J. A. Leary, R. Benz, D. F. Bowersox, C. W. Bjorklund, K. W. R. Johnson, W. J. Maraman, L. J. Mullins and J. G. Reavis, "Pyrometallurigal Purification of Plutonium Reactor Fuels," in *Second United Nations International Conference on the Peaceful Uses of Atomic Energy*, Geneva (Switzerland), 1958.

[4] L. Burris, R. K. Steunenburg and W. E. Miller, "The Application of Electrorefining for Recovery and Purification of Fuel Discharged from the Integral Fast Reactor," in *Annual AIChE Meeting*, Maimi, 1986.

[5] R. W. Benedict, C. Solbrig, B. Westphal, T. A. Johnson, S. X. Li, K. Marsden and K. M. Goff, "Pyroprocessing Progress at Idaho National Laboratory," in *7th International Conference on Advanced Nuclear Fuel Cycles and Systems (GLOBAL 2007)*, Boise, 2007.

[6] H. Lee, J.-M. Hur, J.-G. Kim, D.-H. Ahn, Y.-Z. Cho and S.-W. Paek, "Korean Pyrochemical Process R&D activities," in *Asian Nuclear Prospects 2010,* Daejeon, 2010.

[7] R. Wigeland, T. Bjornard and B. Castle, "The Concept of Goals-Driven Safeguards," Idaho National Laboratory, Idaho Falls, ID, 2009.

[8] R. O. Hoover, "Development of a Computational Model for the Mark-IV Electrorefiner," University of Idaho, Idaho Falls, ID, 2010.

[9] R. D. Mariani and D. Vaden, "Modeled Salt Density for Nuclear Material Estimation in the Treatment of Spent Nuclear Fuel," *Journal of Nuclear Materials,* vol. 404, no. 1, pp. 25-32, 2010.

[10] S. X. Li and M. F. Simpson, "Anodic Process of Electrorefining Spent Driver Fuel in Molten LiCl-KCl-UCl3/Cd System," *Mineral and Metallurgical Processing,* vol. 22, no. 4, p. 192, 2005.

[11] International Atomic Energy Agency, IAEA Safeguards Glossary - 2001 Edition, Vienna: IAEA, 2002.

[12] M. F. Simpson, Interviewee, *Development of New Technology and Methodology for Safeguarding Pyroprocessing.* [Interview]. 6 July 2011.

[13] H. Kim, H. S. Shin and S. K. Ahn, "Status and Prospects of Safeguards By Design for the Pyroprocessing Facility," in *Symposium of International Safeguards*, Vienna, 2010.

[14] P. C. Durst, M. H. Ehinger, B. Boyer, I. Therios, R. Bean, A. Dougan and K. Tolk, "Advanced Safeguards for New TRU Fuel Fabrication Facilities," Pacific Northwest National Laboratory, Richland, WA, 2007.

[15] D. Gerts, M. Paff and R. Bean, "Nuclear Material Accountability Applications of a Continuous Energy and Direction Gamma Ray Detector," in *INMM 51st Annual Meeting*, Baltimore, 2010.

[16] H. E. Garcia, W.-. C. Lin, S. Johnson, T. Burr, S. F. DeMuth, A. J. Bakel, J. K. Krebs and M. H. Ehinger, "Integrated Process Monitoring based on Systems of Sensors for Enhanced Nuclear Safeguards Sensitivity and Robustness," in *52nd INMM Annual Meeting*, Palm Desert, CA, 2011.

[17] R. K. Ahluwalia and T. Q. Hua, "Electrotransport of Uranium from a Liquid Cadmium Anode to a Solid Cathode," *Nuclear Technology*, vol. 140, pp. 41-50, 2002.

[18] P. Zanello, F. Fabrizi de Biani and C. Nervi, Inorganic Electrochemistry:Theory, Practice and Application, 2nd Edition, Cambridge: The Royal Society of Chemistry, 2012.

[19] IUPAC, "Compendium of Chemical Terminology, 2nd ed. (the "Gold Book")," Blackwell Scienitific Publications, 19 August 2012. [Online]. Available: http://goldbook.iupac.org. [Accessed 3 October 2012].

[20] K. Davies and S. X. Li, "Simplified Reference Electrode for Electrorefining of Spent Nuclear Fuel in High Temperature Molten Salt," in *GLOBAL 2007*, Boise, ID, 2007.

[21] K. Scott, Electrochemical Reaction Engineering, San Diego: Academic Press Inc., 1991.

[22] B.-G. Park, "A time-dependent simulation of molten salt electrolysis for nuclear wastes transmutation," Seoul National University, Seoul, South Korea, 1999.

[23] J. Li, M.-S. Yim and D. McNelis, "A Comprehensive Electrorefining Process Simulation Model for Pyroprocessing," in *GLOBAL 2011*, Makuhari, Japan, 2011.

[24] R. Cumberland and M.-S. Yim, "Development of a 1D Transient Electrorefiner Model for Pyroprocess Simulation (Poster)," 2010.

[25] D. Vaden, B. R. Westphal, S. X. Li and T. A. Johnson, "Engineering Scale Liquid Cadmium Cathode Experiments," Idaho National Laboratory, Idaho Falls, ID.

[26] Z. Tomczuk, J. P. Ackerman, R. D. Wolson and W. E. Miller, "Uranium Transport to Solid Electrodes in Pyrochemical Reprocessing of Nuclear Fuel," The Electrochemical Society, Inc., Argonne, IL, 1992.

[27] I. Choi, B. E. Serrano, S. X. Li, S. Herrmann and S. Phongikaroon, "Determination of Exchange Current Density of U3+/U Couple in LiCl-KCl Eutectic Mixture," in *GLOBAL 2009*, Paris, France, 2009.

[28] S. A. Kuznetsov, H. Hayashi, K. Minato and M. Gaune-Escard, "Electrochemical transient techniques for determination of uranium and rare-earth metal separation coefficients in molten salts," *Electrochemical Acta*, vol. 51, pp. 2463-2470, 2006.

[29] R. Cumberland and M.-S. Yim, "Estimation of Uranium and Plutonium Exchange Current Densities on Solid Electrodes," in *International Pyroprocessing Research Conference*, Fontana, WI, 2012.

[30] G. Prentice, Electrochemical Engineering Principles, Englewood Cliffs, NJ: Prentice Hall, 1991.

APPENDICES

Appendix A: Representative Input File and Parameters for PUR and EXCD Studies

---

"Inpref" file for ERAD:

```
 Stage 1 - Continuous electorefining, uranium extraction: RB - 02.11.2009
&input1
  !Temperature (keep at 773 kelvin unless other paramaters are changed accordingly)
    temp=773.d0,
  !Number of elements being tracked in the system
    nelemt=10,
  !Elemtn names (not used, but useful in remembering)
    ename = 'Ur', 'Pu', 'Nd', 'Cd', 'Li', 'Ka', 'Cl', 'Np', 'Na', 'Zr',
  !Standard potentials for each elements (Reverse of conventional sign)
    stde  = 1.248d0, 1.555d0, 0.36d0, 0.635d0, 2.683d0, 2.865d0, -0.895d0, 9.68d0,9.5d0,1.088,
  !Diffusion coefficients in liquid cadmium
    diffu1= 1.51d-5, 1.0d-5,  1.5d-9, 1.5d-5, 1.5d-5, 1.5d-5, 1.5d-5, 1.5d-9, 1.5d-9,1.d-5,
  !Diffusion coefficients in molten salt
    diffu2= 1.45d-5, 1.08d-5, 1d-5, 2.23d-5, 1.13d-5, 2.5d-5, 2.5d-5, 1d-9, 1d-9, 1.13d-5,
  !Standard exchange current densities (A/cm^2)
    curr0 = .5d-4, .5d-4, 5d-9, 5d-9, 5d-9, 5d-9, 5d-9, 5d-9, 5d-9, .5d-4
  !Species valance states
    zi    = 3.000d0, 3.0d0, 3.0d0, 2.00d0, 1.0d0, 1.0d0, -1.0d0, 3.0d0,1.0d0,4.0d0,
  !Transfer coefficient for anode (alpha)
    tca   = 0.400d0, 0.4d0, 0.5d0, 0.50d0, 0.5d0, 0.5d0,  0.5d0,0.5d0,0.5d0,0.4d0,
  !Transfer coefficient for cathode (alpha)
    tcc   = 0.400d0, 0.4d0, 0.5d0, 0.13d0, 0.5d0, 0.5d0,  0.5d0, 0.5d0, 0.5d0, 0.4d0,
  !initial cathode potential (Volts) [-0.5 to -3.0]
    catp=-1.7d0,
  !initial anode potential  (Volts) [-0.5 to -3.0]
    anop=-1.5d0,
  !Number of current 'steps';
    ipset=2,
  !End time of current 'steps' (hours)
    tset= 38.8d0, 38.9d0
  !Current setting for each current 'step' (Amps)
    cmaxt= 100d0, 0.1d0
  !Absolute error for Butler-Volmer Solver (recomended: less than 1d-16)
    aberr=1.d-40,
  !Solubility limit for elements in Cadmium pool (mole fraction)
    psolim =  0.0113d-2, 0.018d-2, 1.0d0, 1.0d0, 1.0d0, 1.0d0, 1.0d0, 1.0d0, 1.0d0, 0.00295d-2
/
&sanode
!Type of solid anode (1=cylinder, 2=cylinder with clad)
  sflag = 2,
!Old input.  Keep it 0
  nempty = 0,
!Number of cells in Zr region
```

```
  nzr = 40,
!Initial mesh cell size in Zr region
  dy2o=1.0d-5,
!Radius of fuel segement
  r0 = 0.254d0,
!Height of fuel segement
  hi0 = 0.635d0,
!Number of chopped fuel segements
  ncfs = 9426,
!Fraction of electrolyte diffusion coefficient in Zr region due to porous media (normally a guess)
  dfrac = .175d0
/
&input2
!Size of anodic liquid metal diffusion layer [keep it the size of 1*dy in this code version] (cm)
  del(1)=1.0d-4,
!Size of anodic molten salt diffusion layer (cm)
  del(2)=5.0d-3,
!Size of cathodic molten salt diffusion layer (cm)
  del(3)=5.0d-3
!Size of cathodic liquid metal diffusion layer [set to 1*dy if solid cathode] (cm)
  del(4)=1.0d-4
!Mesh Size (cm)
    dy=1.0d-4,
!Contact area of anode-salt, cathode-salt, and pool-salt interfaces (cm^2)
  area= 3748.d0,  800.d0
/
&INPUT3
!Solver settings.  Don't mess with them unless you edit the source code.
  ISTATE=1,
  ITASK=5,
  TADD=1.D-3,
  epslon=1.d-5
  iopt=1,
!Maximum number of computations per timestep.  (Has never helped the result)
  mxstep=100,
!First timestep size (seconds).  Keep it small
  h0=0d-15
!Keep this set to 5, which tells lsoda to compute a banded jacobian.
  jt=5,
!Matrix lower bandwidth.  Its minimum value seems to be 19 when using 10 elements.
!Smaller=faster bigger->more stable
!Smaller->faster bigger->more stable
  ml=29,
!Matrix upper bandwidth.  Its minimum value seems to be 19 when using 10 elements.
  mu=29,
  hmax=5.0d1,
  itol=1,
!LSODA/E relative tolerance (I have found it best to keep this number less than 10d-20, but feel
!free to play with it)
  rtoli=1.d-22
!LSODA/E absolute tolerance (This will likely need adjusting.  I have found it should be less than
!1d-6, and preferably beween 1d-10 and 1d-8.  With lsoda, running smaller that 1d-12 causes the code
```

```
!to crash.  With lsode, I have not found a lower limit, but would still reccomend keeping the tolerance
!above 1d-12 for the sake of speed
  atoli=1.d-9
  iprint=2,
/
&input4
!Composition of anode (weight fraction)
 Can= 84.6d-2, .379d-2, 1.0d-9, 1.0d-9, 1.0d-9, 1.0d-9, 1.0d-9, 1.0d-9, 3.55d-2, 11.5d-2,
!Composition of electrolyte (weight fraction)
 Cms=  7.567-2, 0.234d-2, 1.d-9, 1.d-9, 5.95d-2, 22.15d-2, 38.8d-2, 1d-9, 1.52d-2, 1d-9,
!Composition of cathode (weight fraction)
 Cca=  1d-7, 1d-7, 1d-9, 1d-9, 1d-9, 1d-9, 1d-9, 1d-9, 1d-9, 1d-9,
!Composition of pool (weight fraction)
 Cpo=  1.07d-4, 3.05d-6, 1d-9, .999875d-0, 1d-9, 1d-9, 1d-9, 1d-9, 1d-9, 1.53d-3,
!Composition of pool intermetallics (weight fraction)
 Cim=  1d-9, 1d-9, 1d-9, 1d-9, 1d-9, 1d-9, 1d-9, 1d-9, 1d-9, 1d-9,
/
&input5
!masses of anode, electrolyte, cathode, pool, and pool precipitate (cm^3)
  mass= 19.2d3, 447d3, 1d0, 655d3, 1
!Volumes of anode, electrolyte, cathode, pool, and pool precipitate (cm^3)
  vol = 1190d0, 251000d0, 1d0, 78500d0, 1d0
!Atomic weights of the elements
  gatom=238.03,  240.0, 144.24, 112.41, 6.939, 39.1, 35.453, 237.0d0,22.9d0,91.224d0
/
```

Appendix B: Calculation of EXCD

The standard rate constant for the charge transfer of uranium at 773 K is obtained from Table 2 of [28].

$$k_U^o = 2.6 \cdot 10^{-4}\ {}^{cm}/_{s} \tag{B. 1}$$

Using (2.13) and (2.16) with following parameters from [28]:

$$A = 0.165\ cm^2 \tag{B. 2}$$

$$C_{U^{3+}} = 5.68 \cdot 10^{-5}\ {}^{mol}/_{cm^3} \tag{B. 3}$$

Additionally, the remaining parameters are assumed to have the following values:

$$n_U = 3 \tag{B. 4}$$

$$\alpha = 0.4 \tag{B. 5}$$

$$C_{U^{3+}}^o = 1\ {}^{mol}/_{L} = 1 \cdot 10^{-3}\ {}^{mol}/_{cm^3} \tag{B. 6}$$

This results in an exchange current density value of:

$$i_{o,U} = n_U \cdot F \cdot \frac{k^o}{A} \cdot C_{U^{3+}}^{(1-\alpha)} \cdot {C_{U^{3+}}^o}^{\alpha} = 816\ {}^{A}/_{m^2} \tag{B. 7}$$

Appendix C: Plots from EXCD Sensitivity Study

Each plot contains four cases at varying plutonium exchange current density (Pu-EXCD) values. The uranium exchange current density (U-EXCD) and zirconium exchange current density (Zr-EXCD) in each plot are fixed at designated values.

C.1 Plutonium Deposited

C.1.1 U-EXCD = 0.5 A/m^2

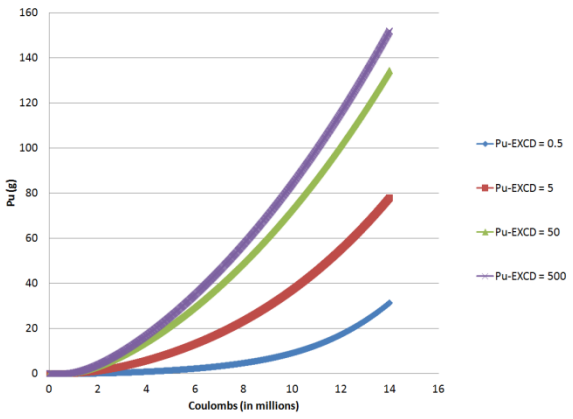

Figure C.1 Zr-EXCD = 0.5 A/m^2

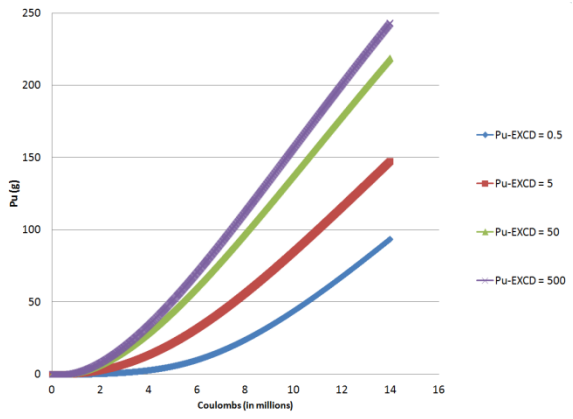

Figure C.2 Zr-EXCD = 5 A/m^2

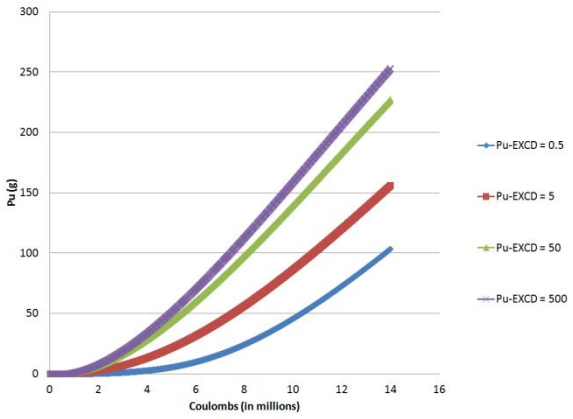

Figure C.3 Zr-EXCD = 50 A/m^2

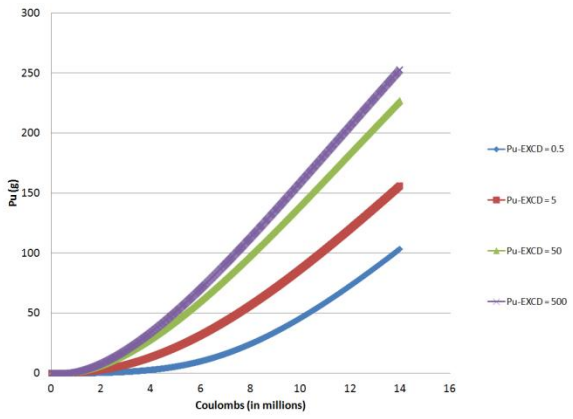

Figure C.4 Zr-EXCD = 500 A/m^2

C.1.2 U-EXCD = 5 A/m^2

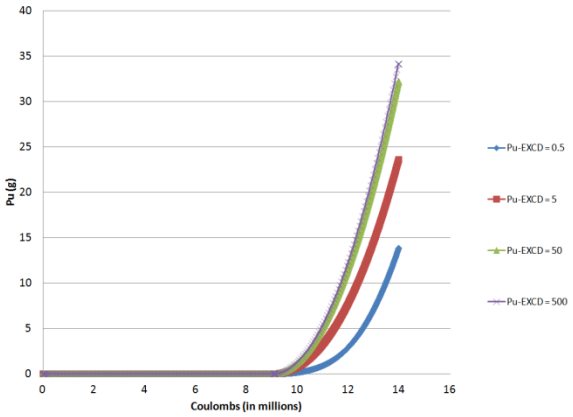

Figure C.5 Zr-EXCD = 0.5 A/m^2

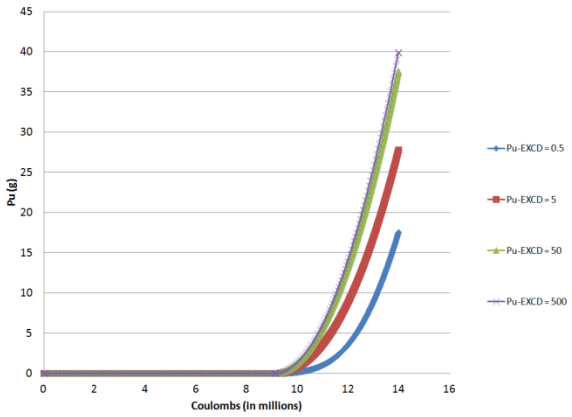

Figure C.6 Zr-EXCD = 5 A/m^2

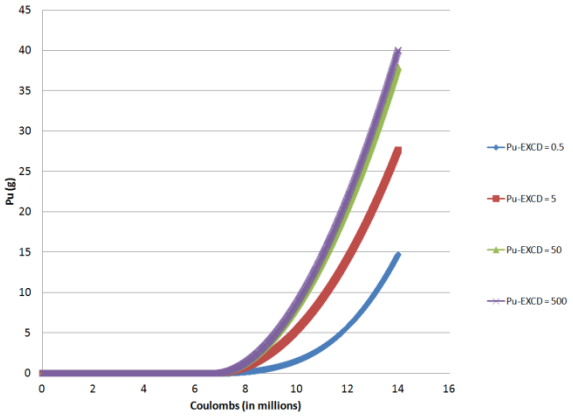

Figure C.7 Zr-EXCD = 50 A/m^2

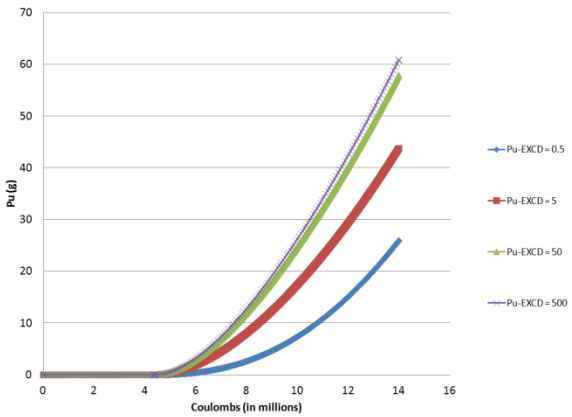

Figure C.8 Zr-EXCD = 500 A/m^2

C.1.3 U-EXCD = 50 A/m^2

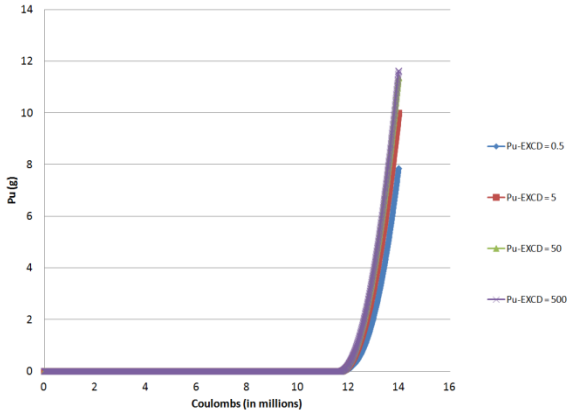

Figure C.9 Zr-EXCD = 0.5 A/m^2

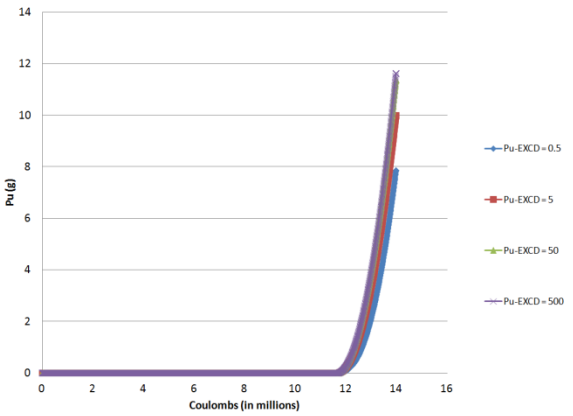

Figure C.10 Zr-EXCD = 5 A/m^2

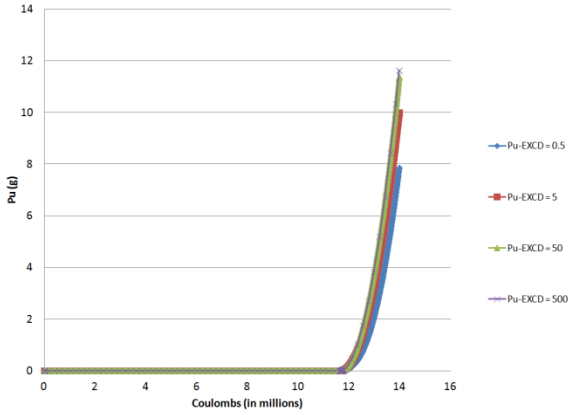

Figure C.11 Zr-EXCD = 50 A/m^2

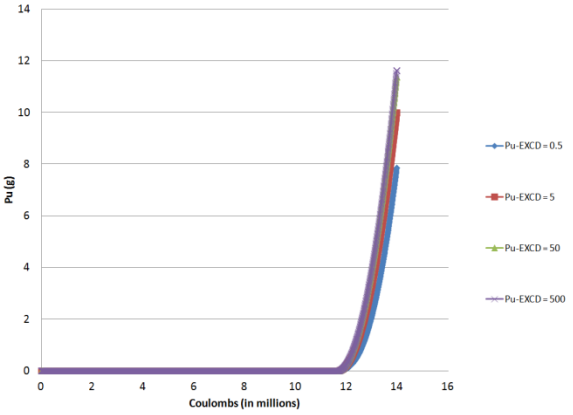

Figure C.12 Zr-EXCD = 500 A/m^2

C.1.4 U-EXCD = 500 A/m^2

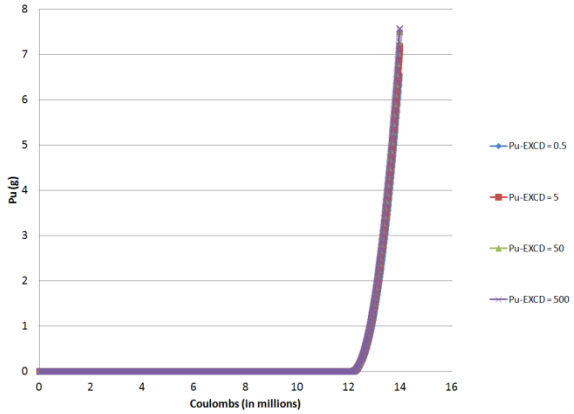

Figure C.13 Zr-EXCD = 0.5 A/m^2

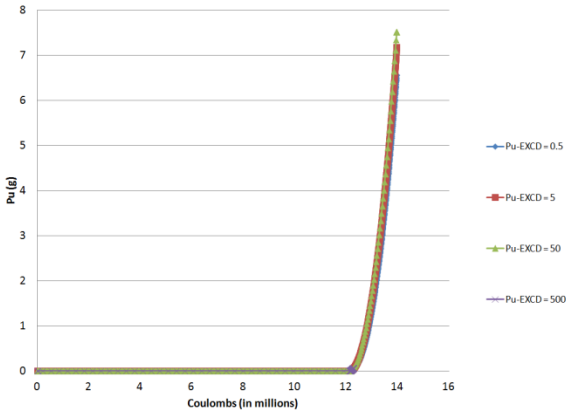

Figure C.14 Zr-EXCD = 5 A/m^2

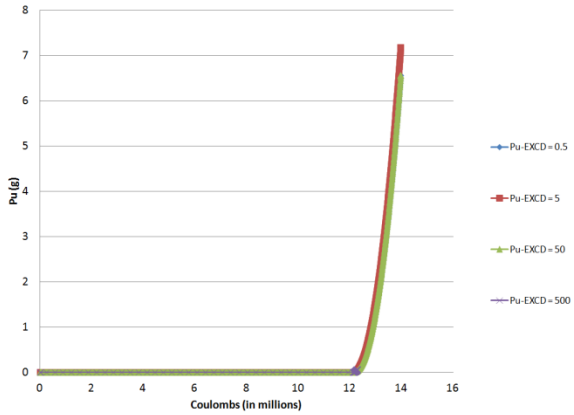

Figure C.15 Zr-EXCD = 50 A/m^2

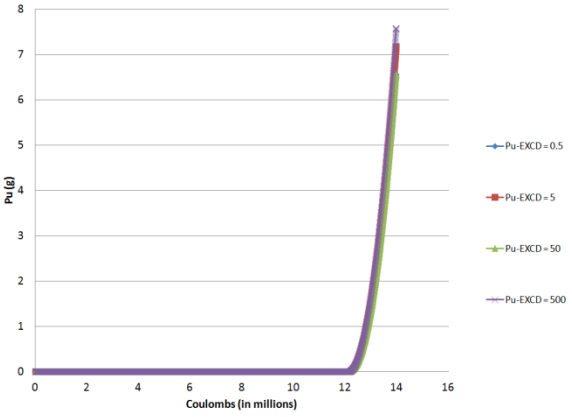

Figure C.16 Zr-EXCD = 500 A/m^2

C.2 Cathode Potential

C.2.1 U-EXCD = 0.5 A/m^2

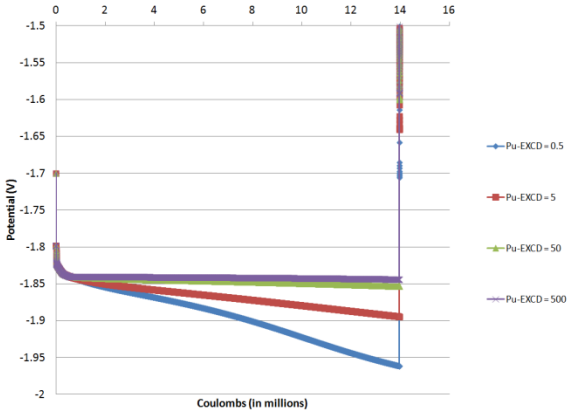

Figure C.17 Zr-EXCD = 0.5 A/m^2

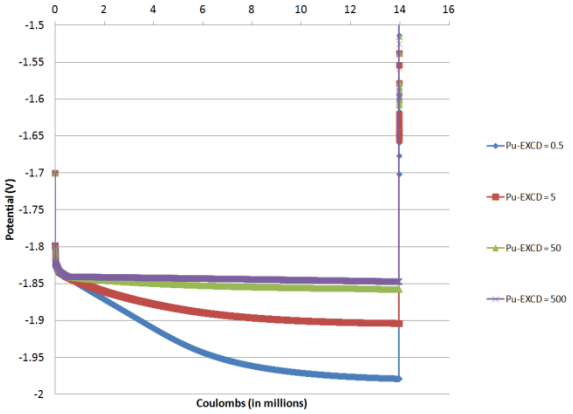

Figure C.18 Zr-EXCD = 5 A/m^2

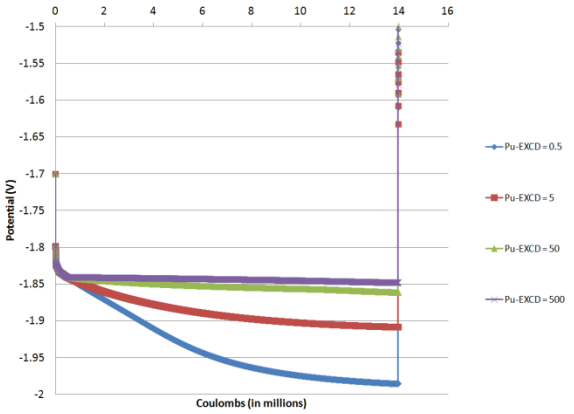

Figure C.19 Zr-EXCD = 50 A/m^2

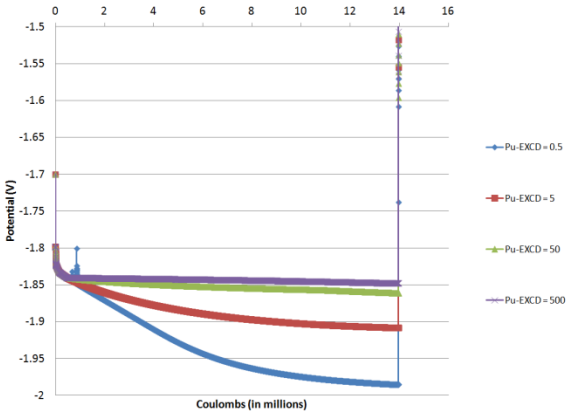

Figure C.20 Zr-EXCD = 500 A/m^2

C.2.2 U-EXCD = 5 A/m^2

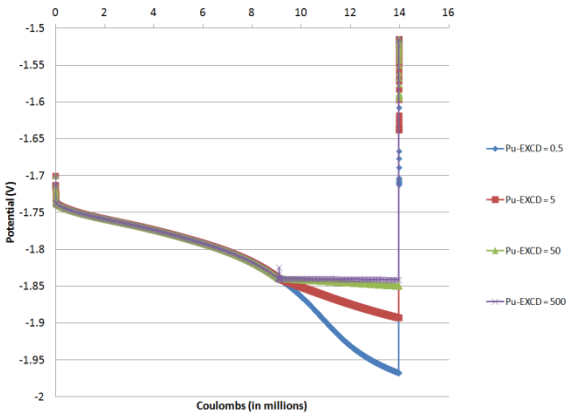

Figure C.21 Zr-EXCD = 0.5 A/m^2

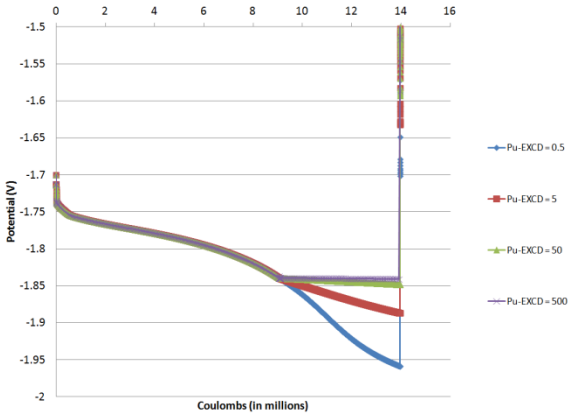

Figure C.22 Zr-EXCD = 5 A/m^2

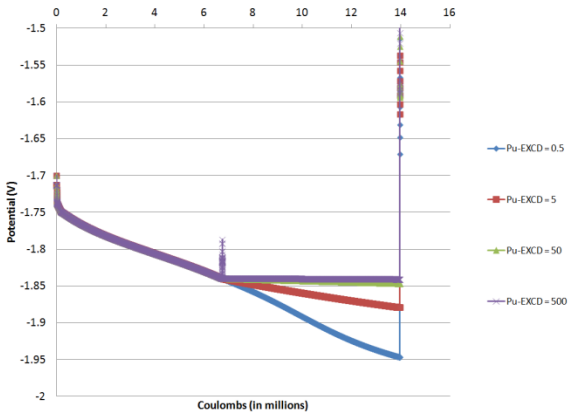

Figure C.23 Zr-EXCD = 50 A/m^2

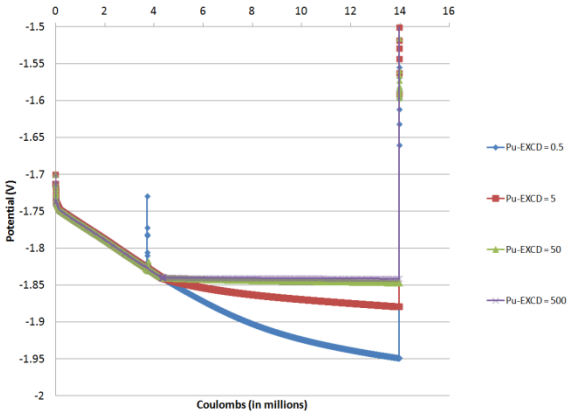

Figure C.24 Zr-EXCD = 500 A/m^2

C.2.3 U-EXCD = 50 A/m^2

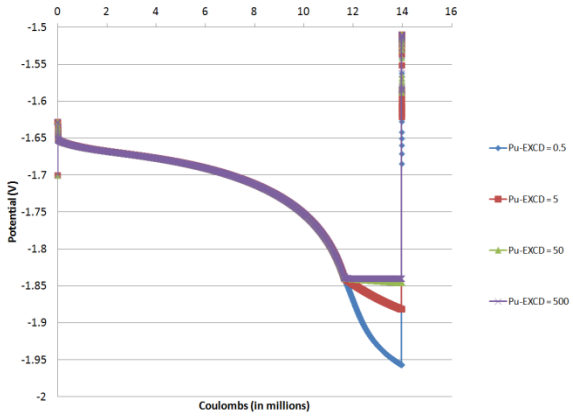

Figure C.25 Zr-EXCD = 0.5 A/m^2

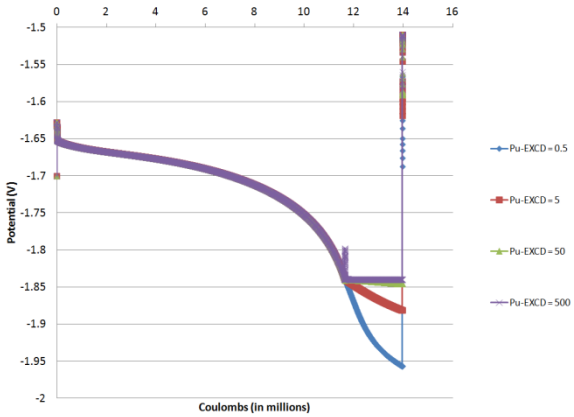

Figure C.26 Zr-EXCD = 5 A/m^2

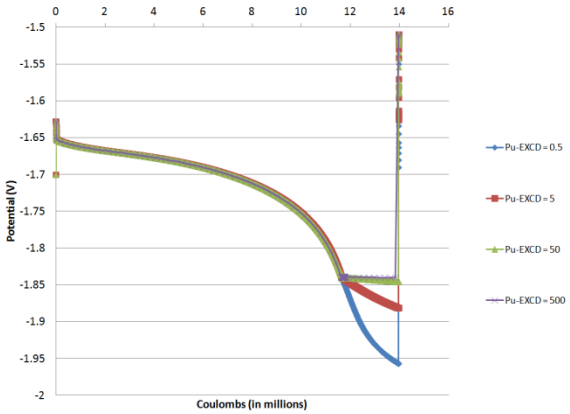

Figure C.27 Zr-EXCD = 50 A/m^2

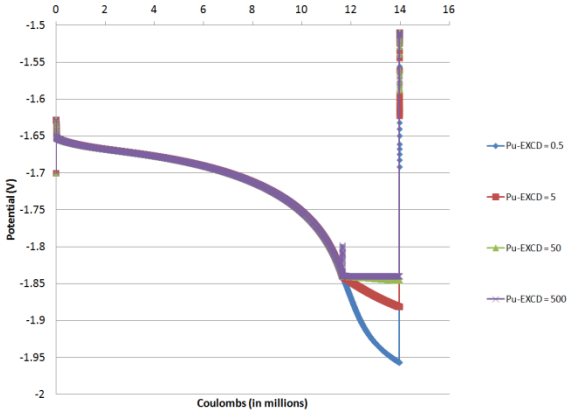

Figure C.28 Zr-EXCD = 500 A/m^2

C.2.4 U-EXCD = 500 A/m^2

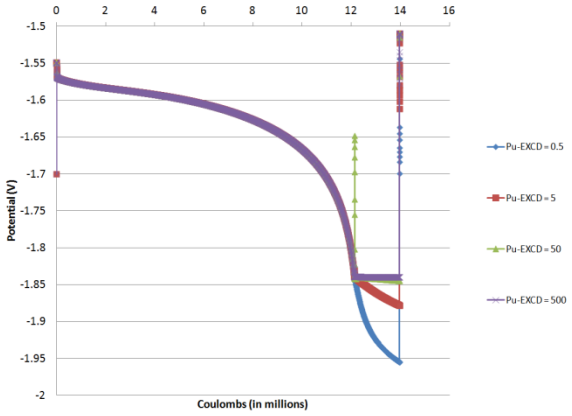

Figure C.29 Zr-EXCD = 0.5 A/m^2

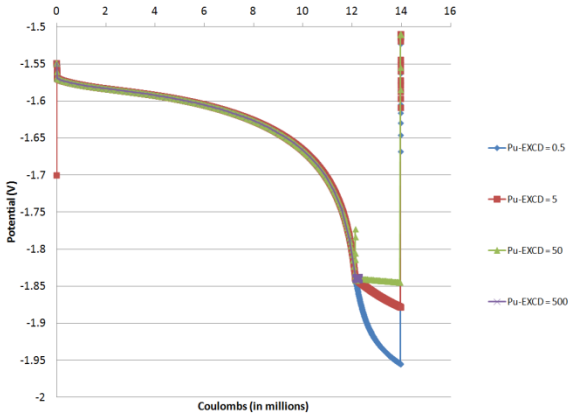

Figure C.30 Zr-EXCD = 5 A/m^2

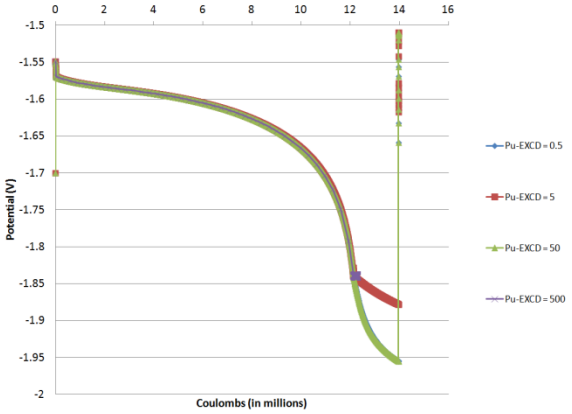

Figure C.31 Zr-EXCD = 50 A/m^2

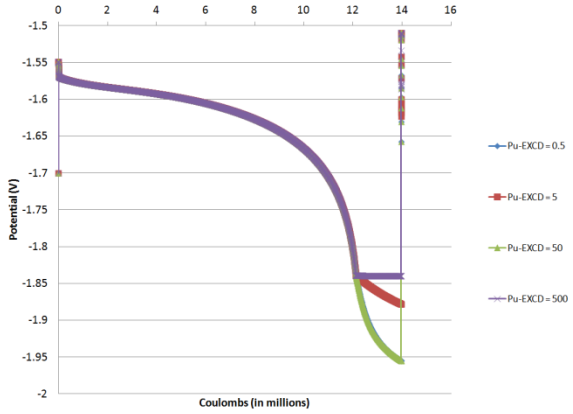

Figure C.32 Zr-EXCD = 500 A/m^2

Appendix D: Abnormal Runs in EXCD Sensitivity Study

U-EXCD	Zr-EXCD	Pu-EXCD	Abnormality
5	0.5	500	Data reduction
5	5	500	Data reduction
5	500	500	Data reduction
50	50	500	Drastic Data Reduction (post-processed twice)
500	0.5	50	Spike at limiting current (convergence issue)
500	0.5	50	Spike at limiting current (convergence issue)
500	5	500	Code crashed at limiting current/Data reduction
500	50	500	Code crashed at limiting current/Data reduction
500	50	50	Copied Pu-EXCD = 0.5 run
500	500	50	Copied Pu-EXCD = 0.5 run

Appendix E: Model User Interface and Code

User-Interface:

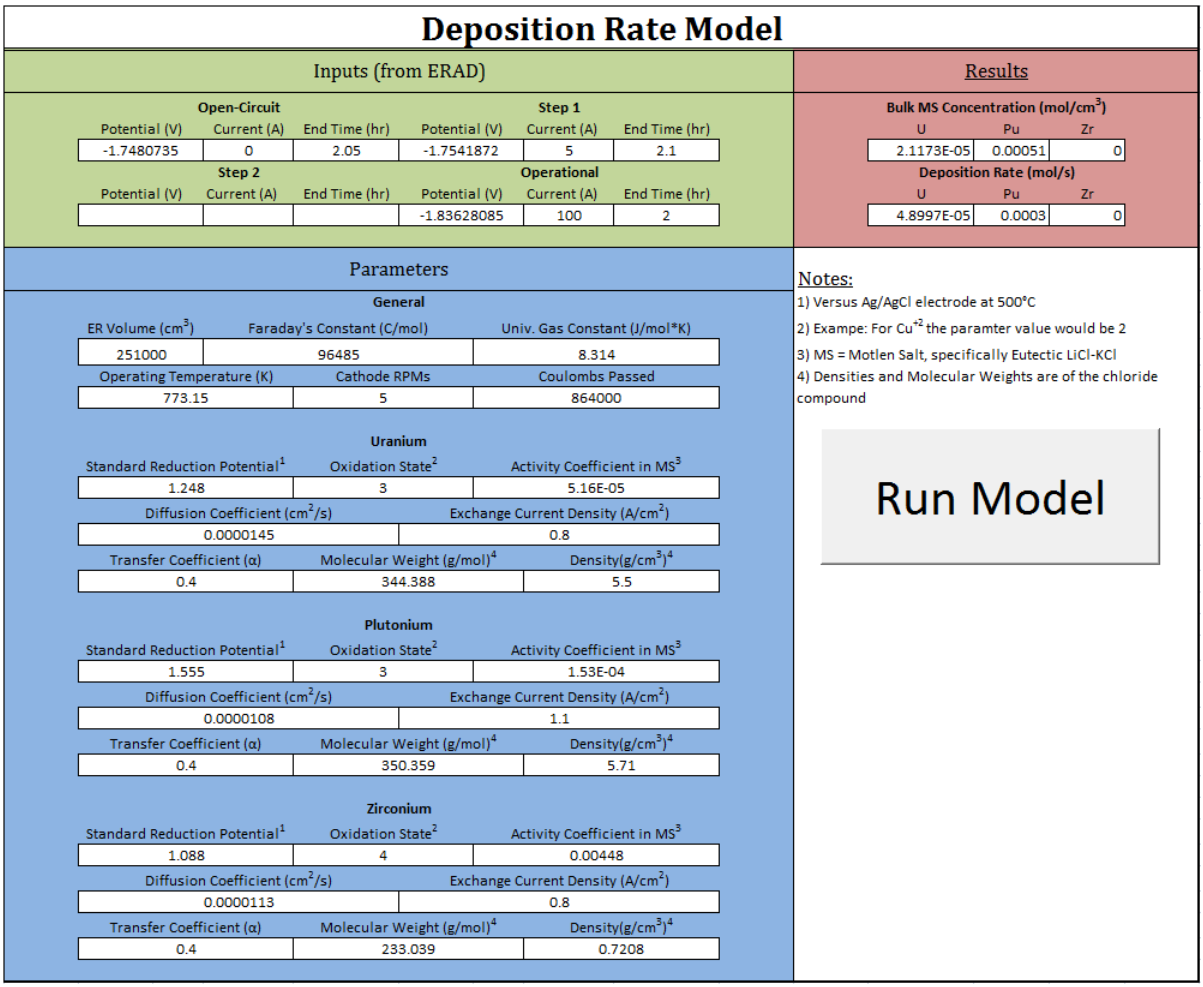

Deposition Rate Model

Inputs (from ERAD)

Open-Circuit			Step 1		
Potential (V)	Current (A)	End Time (hr)	Potential (V)	Current (A)	End Time (hr)
-1.7480735	0	2.05	-1.7541872	5	2.1
Step 2			**Operational**		
Potential (V)	Current (A)	End Time (hr)	Potential (V)	Current (A)	End Time (hr)
			-1.83628085	100	2

Results

Bulk MS Concentration (mol/cm^3)		
U	Pu	Zr
2.1173E-05	0.00051	0
Deposition Rate (mol/s)		
U	Pu	Zr
4.8997E-05	0.0003	0

Parameters

General

ER Volume (cm^3)	Faraday's Constant (C/mol)	Univ. Gas Constant (J/mol*K)
251000	96485	8.314
Operating Temperature (K)	Cathode RPMs	Coulombs Passed
773.15	5	864000

Uranium

Standard Reduction Potential[1]	Oxidation State[2]	Activity Coefficient in MS[3]
1.248	3	5.16E-05
Diffusion Coefficient (cm^2/s)		Exchange Current Density (A/cm^2)
0.0000145		0.8
Transfer Coefficient (α)	Molecular Weight (g/mol)[4]	Density(g/cm^3)[4]
0.4	344.388	5.5

Plutonium

Standard Reduction Potential[1]	Oxidation State[2]	Activity Coefficient in MS[3]
1.555	3	1.53E-04
Diffusion Coefficient (cm^2/s)		Exchange Current Density (A/cm^2)
0.0000108		1.1
Transfer Coefficient (α)	Molecular Weight (g/mol)[4]	Density(g/cm^3)[4]
0.4	350.359	5.71

Zirconium

Standard Reduction Potential[1]	Oxidation State[2]	Activity Coefficient in MS[3]
1.088	4	0.00448
Diffusion Coefficient (cm^2/s)		Exchange Current Density (A/cm^2)
0.0000113		0.8
Transfer Coefficient (α)	Molecular Weight (g/mol)[4]	Density(g/cm^3)[4]
0.4	233.039	0.7208

Notes:

1) Versus Ag/AgCl electrode at 500°C
2) Exampe: For Cu^{+2} the paramter value would be 2
3) MS = Motlen Salt, specifically Eutectic LiCl-KCl
4) Densities and Molecular Weights are of the chloride compound

Run Model

Code:

```
Option Explicit
'Declaring Global Variables
Public E(0 To 3) As Double, I(0 To 3) As Single, Eo(0 To 2) As Single, n(0 To 2) As Single
Public gam(0 To 2) As Single, D(0 To 2) As Single, io(0 To 2) As Single, alp(0 To 2) As Single
Public Vol As Single, F As Single, R As Single, T As Single, Co As Double
Public Isp(0 To 2, 0 To 7) As Double, CA As Single, Cb(0 To 2) As Double
Public Cg(0 To 2) As Double, Sp(0 To 2) As String, ENm(0 To 3) As String, delta As Double
Sub Main()
'"The main subroutine that calls other portions of the code"'
'Declaring Variables
```

```
Dim INm(0 To 3) As String, j As Integer, tol As Double, k As Integer, EPu As Double, EU As Double
Dim init As Boolean, CNT As Integer, NT As Long, diff_new As Double, diff_old As Double
'Turn off screen updates and alerts - enhances speed
Application.ScreenUpdating = False
Application.DisplayAlerts = False

'****PART 1: Reading Inputs & Parameters*****

Sheet1.Activate
'Assinging cell names of Inputs
ENm(0) = "OCP": ENm(1) = "Estep1": ENm(2) = "Estep2": ENm(3) = "Eop"
INm(0) = "OCC": INm(1) = "Istep1": INm(2) = "Istep2": INm(3) = "Iop"
'Read in Inputs from "Inputs" Worksheet
For j = 0 To 3
   E(j) = ThisWorkbook.Names(ENm(j)).RefersToRange
   I(j) = Names(INm(j)).RefersToRange
Next
'Read in Parameters from "Inputs" Worksheet
Vol = Names("ER_Vol").RefersToRange
F = Names("Fa").RefersToRange
R = Names("Rg").RefersToRange
T = Names("Temp").RefersToRange
Sp(0) = "_U": Sp(1) = "_Pu": Sp(2) = "_Zr"
For j = 0 To 2
   Eo(j) = Names("Eo" & Sp(j)).RefersToRange
   n(j) = Names("n" & Sp(j)).RefersToRange
   gam(j) = Names("gam" & Sp(j)).RefersToRange
   D(j) = Names("h" & Sp(j)).RefersToRange
   io(j) = Names("io" & Sp(j)).RefersToRange
   alp(j) = Names("alp" & Sp(j)).RefersToRange
Next
'Additional Parameters
CA = 800 'Cathode area (cm^2)
delta = 0.005 'Diffusion layer thickness (cm)
Co = 0.001 'Standard concentration (mol/cc)
tol = 3 'Convergance tolerance for cell current (A) at operating conditions

'*****PART 2: Finding Solution******

'Test if only uranium deposits on cathode
Cb(0) = Cb_EQ(E(0), 0)
'Cb(species) = Bulk Concentration (mol/cc)
'Species: 0 - Uranium, 1 - Plutonium, 2 - Zirconium
Isp(0, 3) = Curr(E(3), Cb(0), 0, 3)
'Isp(species, step)= Species Current (A)
'Steps: 0 - Open Circuit, 1 - Step 1, 2- Step 2, 3 - Operational
If Abs(Isp(0, 3) - I(3)) < tol Then GoTo 9
'Solve for concentration when U and Pu co-deposit
'GUESSES:
Cb(0) = Cb_EQ(E(0), 0)
Cb(1) = Cb_EQ(E(0), 1)
Cg(0) = Cb(0): Cg(1) = Cb(1)
```

```
'Solve Loop
While Abs(Isp(0, 3) + Isp(1, 3) - I(3)) > tol
   'Initialize difference history
   diff_old = 100
   diff_new = 99
   'Minimizing the difference
   While diff_old > diff_new
      'Solve for side reactant concentration (mol/cc)
      Cg(1) = Cb_S(E(0), Cg(0), 1)
      'Solve for species currents at step 1 (A)
      Isp(0, 1) = Curr(E(1), Cg(0), 0)
      Isp(1, 1) = Curr(E(1), Cg(1), 1)
      'Increment Uranium concentration (mol/cc)
      Cg(0) = Cg(0) + 1 * 10 ^ -8
      'Assign old difference to previous difference
      diff_old = diff_new
      'Determine difference between predicted and measured current at step 1
      diff_new = Abs(Isp(0, 1) + Isp(1, 1) - I(1))
      'Counter to prevent infinite loop
      NT = NT + 1
      If NT = 10 ^ 6 Then Stop
   Wend
   'Determine current at operational conditions
   Isp(0, 3) = Curr(E(3), Cg(0), 0, 3)
   Isp(1, 3) = Curr(E(3), Cg(1), 1, 3)
Wend
'Assign converged solution to concentration array
Cb(0) = Cg(0): Cb(1) = Cg(1)
9
'Populate Results Field
ThisWorkbook.Activate
Sheets("Inputs").Activate
For j = 0 To 2
   Cells(7, 12 + j).Value = Cb(j)
   Cells(10, 12 + j).Value = Isp(j, 3) / F / n(j)
Next
'Re-activate screen updates and alerts
Application.ScreenUpdating = True
Application.DisplayAlerts = True

End Sub

Public Function Cb_EQ(Pot As Double, spec As Integer) As Double
'Determining the bulk concencentration of a species at the Open-Circuit Potential
'Partial solution to the equilibrium potential - Equation 7.1 with eta = 0
Cb_EQ = n(spec) * F / (R * T) * (Pot + Eo(spec))
'Completed solution to equilibrium potential - Equation 7.1
Cb_EQ = Exp(Cb_EQ) * Co / gam(spec)
End Function

Public Function Curr(Pot As Double, C As Double, spec As Integer, Optional step As Integer) As Double
'Determining the current using Butler-Volmer with mass-transport effects – Equation 7.2
```

```
Dim EXP1 As Double, EXP2 As Double, RAT As Double
Dim CuLim As Double, MT As Double, CuBV As Double
'The two exponential terms from Eq. 7.2
EXP1 = Exp(F * n(spec) * (alp(spec) - 1) * (Pot + Eo(spec)) / R / T)
EXP2 = Exp(F * n(spec) * alp(spec) * (Pot + Eo(spec)) / R / T)
'The denominator of the denominator in Eq. 7.2
MT = Co * F * n(spec) * D(spec) / delta
'Species Current from Butler-Volmer equation - Equation 7.2
CuBV = -CA * io(spec) * (EXP2 - gam(spec) * C * EXP1 / Co) / (gam(spec) * io(spec) * EXP1 / MT + 1)
'Limiting Current - Equation 2.23 with a surface concentration of zero
CuLim = n(spec) * F * CA * D(spec) / delta * C
'Check sign of limiting current
If CuBV < 0 Then CuLim = -CuLim
'Assign solution
Curr = CuBV
If Abs(CuBV) > Abs(CuLim) Then Curr = CuLim

End Function
Public Function Cb_S(Pot As Double, CU As Double, spec As Integer) As Double
'Solves for the correlated side reactant concentration given a
'value for the uranium concentration and assuming a two species system
Dim EXP1 As Double, EXP2 As Double, MT As Double
Dim NM1 As Double, NM2 As Double, DNM As Double, Curr_U As Double
'The two exponential terms from Eq. 7.2
EXP1 = Exp(F * n(spec) * (alp(spec) - 1) * (Pot + Eo(spec)) / R / T)
EXP2 = Exp(F * n(spec) * alp(spec) * (Pot + Eo(spec)) / R / T)
'The denominator of the denominator in Eq. 7.2
MT = Co * F * n(spec) * D(spec) / delta
NM1 = EXP1 * io(spec) * gam(spec) / MT + 1
NM2 = CA * EXP2 * io(spec) / NM1
DNM = CA * EXP1 * io(spec) * gam(spec)
'Determine the current of uranium at OCP
Curr_U = Curr(Pot, CU, 0)
'Resulting equation from equating to the negative uranium current at the OCP
Cb_S = Abs(-Co * NM1 * (Curr_U - NM2) / DNM)
End Function
```

Appendix F: Complete Model Results

CASE	1	2	3	4	5	6
Uranium Concentration (mol/cc)						
ERAD	5.26E-04	1.53E-04	1.30E-04	1.33E-04	9.54E-05	9.54E-05
Predicted	5.23E-04	1.55E-04	1.30E-04	1.33E-04	9.85E-05	9.85E-05
Error (%)	0.45%	-1.27%	0.07%	0.04%	-3.27%	-3.23%
Plutonium Concentration (mol/cc)						
ERAD	1.73E-05	1.71E-05	3.99E-05	1.85E-04	1.97E-04	1.97E-04
Predicted	---	---	4.86E-05	1.76E-04	1.75E-04	1.75E-04
Error (%)	---	---	-21.69%	4.99%	11.25%	11.11%
Uranium Deposition Rate (mol/s)						
ERAD	3.45E-04	3.45E-04	3.01E-04	3.04E-04	2.19E-04	2.19E-04
Predicted	3.38E-04	3.52E-04	3.01E-04	3.06E-04	2.28E-04	2.28E-04
Error (%)	2.16%	-2.01%	0.18%	-0.88%	-4.26%	-4.24%
Plutonium Deposition Rate (mol/s)						
ERAD	0.00E+00	0.00E+00	4.44E-05	4.17E-05	1.27E-04	1.27E-04
Predicted	---	---	5.31E-05	3.65E-05	1.08E-04	1.08E-04
Error (%)	---	---	-19.68%	12.60%	14.97%	14.83%

CASE	7	8	9	10	11
Uranium Concentration (mol/cc)					
ERAD	9.65E-05	3.22E-05	2.53E-05	2.54E-05	2.55E-05
Predicted	1.06E-04	2.80E-05	2.13E-05	2.12E-05	2.12E-05
Error (%)	-9.70%	13.21%	16.04%	16.40%	16.85%
Plutonium Concentration (mol/cc)					
ERAD	5.18E-04	2.66E-04	2.65E-04	3.64E-04	4.88E-04
Predicted	4.39E-04	2.87E-04	2.85E-04	3.86E-04	5.11E-04
Error (%)	15.22%	-7.89%	-7.52%	-5.94%	-4.68%
Uranium Deposition Rate (mol/s)					
ERAD	2.18E-04	7.22E-05	5.64E-05	5.59E-05	5.55E-05
Predicted	2.44E-04	6.48E-05	4.93E-05	4.92E-05	4.90E-05
Error (%)	-11.76%	10.27%	12.64%	12.02%	11.66%
Plutonium Deposition Rate (mol/s)					
ERAD	1.27E-04	2.73E-04	2.89E-04	2.90E-04	2.90E-04
Predicted	1.01E-04	2.87E-04	3.02E-04	2.98E-04	2.96E-04
Error (%)	20.99%	-4.89%	-4.58%	-3.02%	-2.03%